Interpreting A and B-metrics with Λ as gravitational field of a tachyon in (anti-)de Sitter universe

O. Hruška[1*] and J. Podolský[1†]

[1]Institute of Theoretical Physics, Charles University,
V Holešovičkách 2, 18000 Prague 8, Czech Republic.

August 13, 2018

Abstract

We investigate main properties and mutual relations of the so-called A and B-metrics with any value of the cosmological constant. In particular, we explicitly show that both the AII and BI-metrics are, in fact, the famous Schwarzschild–(anti-)de Sitter spacetime (that is the AI-metric) boosted to superluminal speed. Together they form the complete gravitational field of a tachyon in Minkowski or (anti-)de Sitter universe. The boundary separating the AII and BI regions is the Mach–Cherenkov shockwave on which the curvature is unbounded. We analyze various geometric features of such spacetimes, we provide their natural physical interpretation, and we visualize them using convenient background coordinates and embeddings.

*E–mail: HruskaOndrej(at)seznam.cz
†E–mail: podolsky(at)mbox.troja.mff.cuni.cz

1 Introduction

In a seminal work [1] published in 1962, J. Ehlers and W. Kundt systematically investigated static vacuum gravitational fields. In particular, they introduced a classification of all such fields of algebraic type D, denoting them as classes A and B (and also C, later interpreted physically as the metric in a static region around uniformly accelerating black holes [2]).

The A-metrics, consisting of three subclasses, were written in [1] in the form[1]

$$AI: \quad \mathrm{d}s^2 = r^2\left(\mathrm{d}\vartheta^2 + \sin^2\vartheta\,\mathrm{d}\varphi^2\right) + \left(1-\frac{b}{r}\right)^{-1}\mathrm{d}r^2 - \left(1-\frac{b}{r}\right)\mathrm{d}t^2\,, \tag{1}$$

$$AII: \quad \mathrm{d}s^2 = z^2\left(\mathrm{d}r^2 + \sinh^2 r\,\mathrm{d}\varphi^2\right) + \left(\frac{b}{z}-1\right)^{-1}\mathrm{d}z^2 - \left(\frac{b}{z}-1\right)\mathrm{d}t^2\,, \tag{2}$$

$$AIII: \quad \mathrm{d}s^2 = z^2\left(\mathrm{d}r^2 + r^2\,\mathrm{d}\varphi^2\right) + z\,\mathrm{d}z^2 - \frac{\mathrm{d}t^2}{z}\,, \tag{3}$$

see also Table 18.2 in [3] or Chapter 9 in [4]. The AI-metric is the famous Schwarzschild solution [5] describing external vacuum field of a spherically symmetric static object or black hole. The A-metrics can be generalized to include (for example) a cosmological constant Λ, and can be written in a unified form

$$\mathrm{d}s^2 = p^2(\epsilon_0 - \epsilon_2\,q^2)\,\mathrm{d}\varphi^2 + \frac{p^2}{\epsilon_0-\epsilon_2\,q^2}\,\mathrm{d}q^2 - \left(\epsilon_2 + \frac{2n}{p} - \frac{\Lambda}{3}\,p^2\right)\mathrm{d}t^2 + \left(\epsilon_2 + \frac{2n}{p} - \frac{\Lambda}{3}\,p^2\right)^{-1}\mathrm{d}p^2\,. \tag{4}$$

For $\epsilon_2 = 1, -1, 0$, we obtain the AI, AII and $AIII$-metric, respectively, as indicated in Table 1. The AI-metric with Λ is the (so called) Schwarzschild–de Sitter solution, first found by Kottler [6], its standard form is obtained by $p = r$, $q = \cos\vartheta$, $n = -m$, $\epsilon_0 = 1$. The AII and $AIII$-metrics have been described and studied as "topological black holes" (see, e.g., [4] for the list of references).

The B-metrics were introduced in [1] in the form

$$BI: \quad \mathrm{d}s^2 = \left(1-\frac{b}{r}\right)^{-1}\mathrm{d}r^2 + \left(1-\frac{b}{r}\right)\mathrm{d}\varphi^2 + r^2\left(\mathrm{d}\vartheta^2 - \sin^2\vartheta\,\mathrm{d}t^2\right), \tag{5}$$

$$BII: \quad \mathrm{d}s^2 = \left(\frac{b}{z}-1\right)^{-1}\mathrm{d}z^2 + \left(\frac{b}{z}-1\right)\mathrm{d}\varphi^2 + z^2\left(\mathrm{d}r^2 - \sinh^2 r\,\mathrm{d}t^2\right), \tag{6}$$

$$BIII: \quad \mathrm{d}s^2 = z\,\mathrm{d}z^2 + \frac{\mathrm{d}\varphi^2}{z} + z^2\left(\mathrm{d}r^2 - r^2\mathrm{d}t^2\right). \tag{7}$$

Although these metrics also look very simple and have been known for more than fifty years, they have been paid much less attention than their counterparts (1)–(3). Analogously to (4), it is possible to include any cosmological constant and write the B-metrics in a unified form

$$\mathrm{d}s^2 = -p^2(\epsilon_0 - \epsilon_2\,q^2)\,\mathrm{d}t^2 + \frac{p^2}{\epsilon_0-\epsilon_2\,q^2}\,\mathrm{d}q^2 + \left(\epsilon_2 + \frac{2n}{p} - \frac{\Lambda}{3}\,p^2\right)\mathrm{d}z^2 + \left(\epsilon_2 + \frac{2n}{p} - \frac{\Lambda}{3}\,p^2\right)^{-1}\mathrm{d}p^2\,. \tag{8}$$

For the choice $\epsilon_2 = 1, -1, 0$, we obtain the BI, BII and $BIII$-metric, respectively, as also summarized in Table 1. Moreover, as we demonstrated in [7,8], the parameter $\epsilon_0 = 1, -1, 0$ has *no physical meaning* because it only changes specific coordinate foliation of the two-dimensional subspace covered by the t and q coordinates. Without loss of generality we may thus choose any ϵ_0 to obtain the most suitable form of the metric.

[1] We distinguish three types of the A and B-metrics by roman numbers, instead of arabic employed in [1].

	ϵ_2	ϵ_0	φ	q	t	p	n	Equations
AI	1	1	φ	$\cos\vartheta$	t	r	$-b/2$	(4) $\to$ (1)
AII	-1	-1	φ	$\cosh r$	t	z	$b/2$	(4) $\to$ (2)
$AIII$	0	1	$r\sin\varphi$	$r\cos\varphi$	t	z	$1/2$	(4) $\to$ (3)
			t	q	z	p	n	Equations
BI	1	1	t	$\cos\vartheta$	φ	r	$-b/2$	(8) $\to$ (5)
BII	-1	-1	t	$\cosh r$	φ	z	$b/2$	(8) $\to$ (6)
$BIII$	0	1	$r\sinh t$	$r\cosh t$	φ	z	$1/2$	(8) $\to$ (7)

Table 1: Transformations between the unified form (4) of A-metrics (upper part) or B-metrics (8) (lower part) and the original forms (1)–(3) or (5)–(7), respectively, as presented by Ehlers and Kundt in the case when $\Lambda = 0$.

The A-metric (4) can further be generalized to include electromagnetic charges, rotation, NUT parameter, and acceleration. Such generalized black holes are contained in the large Plebański–Demiański class [9] of *expanding* type D solutions, see [10] for more details. Interestingly, the C-metric is then also naturally included in this Plebański–Demiański class.

Moreover, the B-metrics can also be considered as a subcase of the Plebański–Demiański class of metrics in a *non-expanding* limit in which the double degenerate null congruence has zero expansion, shear and twist. Such class has the form

$$\mathrm{d}s^2 = \varrho^2\Big(-\mathcal{Q}\,\mathrm{d}t^2 + \frac{1}{\mathcal{Q}}\,\mathrm{d}q^2\Big) + \frac{\mathcal{P}}{\varrho^2}\Big(\mathrm{d}z + 2\gamma q\,\mathrm{d}t\Big)^2 + \frac{\varrho^2}{\mathcal{P}}\,\mathrm{d}p^2, \tag{9}$$

where

$$\begin{aligned} \varrho^2 &= p^2 + \gamma^2\,, \qquad \mathcal{Q}(q) = \epsilon_0 - \epsilon_2\,q^2\,, \\ \mathcal{P}(p) &= \big(-(e^2+g^2) - \epsilon_2\gamma^2 + \Lambda\gamma^4\big) + 2n\,p + (\epsilon_2 - 2\Lambda\gamma^2)\,p^2 - \tfrac{1}{3}\Lambda\,p^4\,, \end{aligned} \tag{10}$$

see Section 16.4 in [4]. It contains two discrete geometrical parameters $\epsilon_0, \epsilon_2 = 1, -1, 0$, the cosmological constant Λ, electric and magnetic charges e and g, mass-like parameter n, and additional parameter γ. A thorough investigation of the corresponding de Sitter and anti-de Sitter "backgrounds" in the form (9) (when $n, \gamma, e, g = 0$, with $\Lambda \neq 0$) was performed in [7,11]. The Minkowski "background" with $\Lambda = 0$, and physical meaning of all seven independent parameters of (9), have been recently clarified in [8]. Clearly, by setting $e, g, \gamma = 0$, the class of metrics (9), (10) reduces to the B-metrics (8).

For both A and B-metrics (4) and (8), the only nonzero Weyl curvature NP scalar is

$$\Psi_2 = \frac{n}{p^3}\,, \tag{11}$$

see [8]. The metrics are thus of algebraic type D (or conformally flat when $n = 0$) and have a curvature singularity at $p = 0$. Since the metrics depend on the fraction n/p, we may restrict ourselves to $p > 0$ while keeping n arbitrary. In order to keep the signature $(-,+,+,+)$, we must also constraint the range of p such that $\mathcal{P}(p) > 0$.

As noted already by Ehlers and Kundt in [1], the A-metrics (4) and the B-metrics (8) have very similar forms, formally related by a complex transformation $\varphi = \mathrm{i}\,t$ and $t = \mathrm{i}\,z$, implying

$\mathrm{d}\varphi^2 \to -\mathrm{d}t^2$ and $\mathrm{d}t^2 \to -\mathrm{d}z^2$. However, this seems to be just a "heuristic trick", a specific kind of "Wick rotation". It is preferable to avoid such a formal identification. Instead, following [12], in Section 2 we will employ a different approach to relate the A and B-metrics. This will be based on performing a *boost of the source*, a procedure more acceptable from the physical point of view. In Section 3 we will investigate the admitted coordinate ranges and possible extensions of the B-metrics. Subsequently, in Section 4 we will examine main geometrical properties of the complete gravitational fields of a tachyonic source, composed of the AII and BI-metrics, with the Mach–Cherenkov shocks. All these results will then be generalized to any value of the cosmological constant Λ in Sections 5–7.

2 AII and BI-metrics are the Schwarzschild spacetime boosted to infinite speed

In 1970, A. Peres [12] realized that it is possible to obtain exact gravitational field of a (hypothetical) tachyon by boosting the classic Schwarzschild source (written in isotropic coordinates) to superluminal speed. In fact, by this procedure the Mach–Cherenkov shock-wave is also generated which separates two distinct regions which are described by the AII and BI-metrics. Such tachyonic counterparts of the Schwarzschild black hole solution were subsequently studied in more detail by L. S. Schulman [13] and J. R. Gott [14]. Let us first summarize this procedure by explicitly "boosting" the usual form of the Schwarzschild metric to infinite speed, obtaining thus the gravitational field of a tachyon. And vice versa: It is possible to "slow-down" the tachyonic source of the AII and BI-metrics to zero speed, obtaining thus the usual Schwarzschild AI-metric of a static source. In this sense, the AI, AII and BI-metrics are related and, in fact, "equivalent" — they just represent (various regions) of the graviational field generated by a massive source moving with all possible velocities, including zero and infinity.

2.1 Boosting the Schwarzschild (AI-)metric to $v \to \infty$

The Schwarzschild metric in the form (4) with $\epsilon_2 = 1 = \epsilon_0$, $\Lambda = 0$, $n = -m$ can be written in Cartesian coordinates

$$p = r = \sqrt{X^2+Y^2+Z^2}\,, \qquad q = \cos\vartheta = \frac{Z}{\sqrt{X^2+Y^2+Z^2}}\,, \qquad \tan\varphi = \frac{Y}{X}\,, \qquad T = t\,, \tag{12}$$

as

$$\begin{aligned} \mathrm{d}s^2 = &-\mathrm{d}T^2 + \mathrm{d}X^2 + \mathrm{d}Y^2 + \mathrm{d}Z^2 \\ &+\frac{2m}{\sqrt{X^2+Y^2+Z^2}}\left(\mathrm{d}T^2 + \left(1-\frac{2m}{\sqrt{X^2+Y^2+Z^2}}\right)^{-1}\frac{(X\mathrm{d}X+Y\mathrm{d}Y+Z\mathrm{d}Z)^2}{X^2+Y^2+Z^2}\right). \end{aligned} \tag{13}$$

Let us now perform a boost in the Z-direction:

$$T = \frac{T' + v\,Z'}{\sqrt{1-v^2}}, \qquad Z = \frac{Z' + v\,T'}{\sqrt{1-v^2}}\,. \tag{14}$$

Although this boost is only allowed for velocities $|v| < 1$, it is interesting to observe that *all terms in the metric* (13) *that introduce* $\sqrt{1-v^2}$ *via* T *and* Z *are quadratic*. It is thus possible

to consider the limit $v \to \infty$, resulting in

$$\lim_{v\to\infty} T^2 = \lim_{v\to\infty} \frac{(T' + v\,Z')^2}{1-v^2} = -Z'^2\,, \qquad \lim_{v\to\infty} Z^2 = \lim_{v\to\infty} \frac{(Z' + v\,T')^2}{1-v^2} = -T'^2\,. \tag{15}$$

The "infinite boost" thus effectively causes *just a swap* $T^2 \to -Z'^2$ and $Z^2 \to -T'^2$, so that the exact Schwarzschild metric (13) becomes

$$\begin{aligned} \mathrm{d}s^2 &= -\mathrm{d}T'^2 + \mathrm{d}X^2 + \mathrm{d}Y^2 + \mathrm{d}Z'^2 \\ &+\frac{2m}{\sqrt{-T'^2+X^2+Y^2}}\left(-\,\mathrm{d}Z'^2 + \left(1-\frac{2m}{\sqrt{-T'^2+X^2+Y^2}}\right)^{-1}\frac{(-T'\mathrm{d}T' + X\mathrm{d}X + Y\mathrm{d}Y)^2}{-T'^2+X^2+Y^2}\right). \end{aligned} \tag{16}$$

In fact, this is the AII-metric in the region $T'^2 > Y^2 + Z^2$ for m purely imaginary, and the BI-metric in the complementary region $T'^2 < Y^2 + Z^2$ for m real.

Indeed, the AII-metric (4) with $\epsilon_2 = -1 = \epsilon_0$, $\Lambda = 0$, written in Cartesian coordinates

$$p = \sqrt{T^2 - X^2 - Y^2}\,, \qquad q = \frac{T}{\sqrt{T^2 - X^2 - Y^2}}\,, \qquad \tan\varphi = \frac{Y}{X}\,, \qquad t = Z\,, \tag{17}$$

reads

$$\begin{aligned} \mathrm{d}s^2 &= -\mathrm{d}T^2 + \mathrm{d}X^2 + \mathrm{d}Y^2 + \mathrm{d}Z^2 \\ &+\frac{2n}{\sqrt{T^2-X^2-Y^2}}\left(-\,\mathrm{d}Z^2 + \left(1-\frac{2n}{\sqrt{T^2-X^2-Y^2}}\right)^{-1}\frac{(-T\mathrm{d}T + X\mathrm{d}X + Y\mathrm{d}Y)^2}{-T^2+X^2+Y^2}\right). \end{aligned} \tag{18}$$

This is exactly the boosted Schwarzschild metric (16) with the identification $m = \mathrm{i}\,n$, i.e. for purely imaginary mass of the (necessarily tachyonic) source. Here we consider the principal square root $\sqrt{-T'^2+X^2+Y^2} = \mathrm{i}\sqrt{T'^2-X^2-Y^2}$. Of course, the transformation (17) is only valid in the region $T^2 > X^2 + Y^2$.

Similarly, the BI-metric (8) with $\epsilon_2 = 1$, $\epsilon_0 = -1$ (which is a more convenient coordinate representation than $\epsilon_0 = 1$), $\Lambda = 0$ is put to Cartesian coordinates in the region $T^2 < X^2 + Y^2$ by

$$p = \sqrt{-T^2 + X^2 + Y^2}\,, \qquad q = \frac{T}{\sqrt{-T^2+X^2+Y^2}}\,, \qquad \tan t = \frac{Y}{X}\,, \qquad z = Z\,, \tag{19}$$

taking the form

$$\begin{aligned} \mathrm{d}s^2 &= -\mathrm{d}T^2 + \mathrm{d}X^2 + \mathrm{d}Y^2 + \mathrm{d}Z^2 \\ &-\frac{2n}{\sqrt{-T^2+X^2+Y^2}}\left(-\,\mathrm{d}Z^2 + \left(1+\frac{2n}{\sqrt{-T^2+X^2+Y^2}}\right)^{-1}\frac{(-T\mathrm{d}T + X\mathrm{d}X + Y\mathrm{d}Y)^2}{-T^2+X^2+Y^2}\right). \end{aligned} \tag{20}$$

Again, this is exactly the boosted Schwarzschild metric (16), in this case directly with $m = -n$.

2.2 Slowing the AII-metric to $v \to 0$

Of course, it is also possible to consider a complementary procedure. Instead of boosting the Schwarzschild static source to infinite speed, we can stop the tachyonic source of the AII-metric. This is achieved by performing the boost[2]

$$T = \frac{v\,T' - Z'}{\sqrt{v^2-1}}\,, \qquad Z = \frac{v\,Z' - T'}{\sqrt{v^2-1}}\,. \tag{21}$$

[2]This is formally the same as (14) for v replaced by $-1/v$.

of the metric (18). Although (21) is only allowed for $v > 1$, the metric is quadratic in T and Z, so that it is possible to make the limit $v \to 0$, resulting in

$$\lim_{v\to 0} T^2 = \lim_{v\to 0} \frac{(v\,T' - Z')^2}{v^2-1} = -Z'^2\,, \qquad \lim_{v\to 0} Z^2 = \lim_{v\to 0} \frac{(v\,Z' - T')^2}{v^2-1} = -T'^2\,. \tag{22}$$

As in the case (15), the limit $v \to 0$ causes the swap $T^2 \to -Z'^2$ and $Z^2 \to -T'^2$. The AII-metric (18), valid in $T^2 > X^2 + Y^2$, slowed down to $v = 0$ is thus

$$\begin{aligned} \mathrm{d}s^2 &= -\mathrm{d}T'^2 + \mathrm{d}X^2 + \mathrm{d}Y^2 + \mathrm{d}Z'^2 \\ &+\frac{2n}{\sqrt{-X^2-Y^2-Z'^2}}\left(\mathrm{d}T'^2 + \left(1 - \frac{2n}{\sqrt{-X^2-Y^2-Z'^2}}\right)^{-1} \frac{(X\mathrm{d}X + Y\mathrm{d}Y + Z'\mathrm{d}Z')^2}{X^2+Y^2+Z'^2}\right). \end{aligned} \tag{23}$$

In the region $X^2 + Y^2 + Z'^2 > 0$ this is the Schwarzschild metric (13) with $n = \mathrm{i}\,m$.

2.3 Slowing the BI-metric to $v \to 0$

Using the boost (21) we can similarly stop the superluminal tachyonic source of the BI-metric. Due to the swap (22), the metric (20) valid in the region $T^2 < X^2 + Y^2$ becomes

$$\begin{aligned} \mathrm{d}s^2 &= -\mathrm{d}T'^2 + \mathrm{d}X^2 + \mathrm{d}Y^2 + \mathrm{d}Z'^2 \\ &-\frac{2n}{\sqrt{X^2+Y^2+Z'^2}}\left(\mathrm{d}T'^2 + \left(1 + \frac{2n}{\sqrt{X^2+Y^2+Z'^2}}\right)^{-1} \frac{(X\mathrm{d}X + Y\mathrm{d}Y + Z'\mathrm{d}Z')^2}{X^2+Y^2+Z'^2}\right), \end{aligned} \tag{24}$$

that is the Schwarzschild metric (13) in the region $X^2 + Y^2 + Z'^2 > 0$, simply relabeling $m = -n$.

Both the AII and BI-metrics can thus be physically interpreted as (a formal limit of) the Schwarzschild solution boosted to an infinite speed. And vice versa: the superluminal sources of the AII and BI-metrics can be slowed down and even stopped, yielding exactly the classic Schwarzschild metric of a static massive source. In this sense, all these three exact metrics can be understood as representing the "same gravitational field", the *distinction given only by the speed of the source* and the *region* of spacetime covered by the corresponding coordinates.

It can also be seen than in the weak-field limit $n \to 0$, the AII-metric (18) and the BI-metric (20) *together cover the whole Minkowski spacetime*, except the "separation boundary" surface $T^2 = X^2 + Y^2$ between them. Physically, it identifies the *Mach–Cherenkov shock wave* which will be described in more detail in Section 4, and extended to any value of the cosmological constant Λ in Section 7.

3 Coordinate ranges and extensions of the B-metrics

It is now important to investigate the admitted coordinate ranges of the B-metrics, and their analytic extensions. We start with the case $\Lambda = 0$, more general B-metrics with a cosmological constant Λ will be described in Section 6.

3.1 The BI-metric

The BI-metric is given by (8) with $\epsilon_2 = 1$, $\Lambda = 0$, that is

$$\mathrm{d}s^2 = -p^2(\epsilon_0 - q^2)\,\mathrm{d}t^2 + \frac{p^2}{\epsilon_0 - q^2}\,\mathrm{d}q^2 + \Big(1 + \frac{2n}{p}\Big)\mathrm{d}z^2 + \Big(1 + \frac{2n}{p}\Big)^{-1}\mathrm{d}p^2\,. \tag{25}$$

Here $z \in \mathbb{R}$, while the range of t, q depends on ϵ_0. Ehlers and Kundt in [1] considered the case $\epsilon_0 = 1$, see Table 1. Due to (11), the range of p in (25) depends on the sign of n. For $n > 0$ it is $p \in (0, \infty)$, with a curvature singularity at $p = 0$, while for $n < 0$ it is $p \in (2|n|, \infty)$. Ehlers and Kundt suggested a possible analytic extension of the BI-metric with $n < 0$ across $p = 2|n|$ in the p-coordinate. For the choice $\epsilon_0 = -1$, this is achieved by the transformation[3]

$$p = 2|n|/(1 - \rho^2)\,, \qquad q = \sinh\tau\,, \qquad z = 2n\,\zeta\,, \qquad t = \varphi\,, \tag{26}$$

which puts the metric (25) into the form

$$\mathrm{d}s^2 = 4n^2\Big[\big(1-\rho^2\big)^{-2}\big(-\mathrm{d}\tau^2 + \cosh^2\tau\,\mathrm{d}\varphi^2\big) + \rho^2\mathrm{d}\zeta^2 + 4\big(1-\rho^2\big)^{-4}\mathrm{d}\rho^2\Big]\,, \tag{27}$$

see metric (2–3.47) in [1]. Although the term $\rho^2\mathrm{d}\zeta^2$ vanishes at $\rho = 0$, there is *no singularity*. The coordinates (27) of the BI-metric thus better illustrate the behaviour of the spacetime. At $\rho = 0$, corresponding to $p = 2|n|$, the curvature (11) reaches its *maximal but finite value* (in fact, it is impossible to reach the curvature singularity located at $p = 0$). It is now straightforward to extend the range of ρ to *negative values*, so that $\rho \in (-1, 1)$. With $\rho \to \pm 1$ the spacetime becomes asymptotically flat (since $p \to \infty$). In this aspect, the global structure of the BI-metric resembles the famous Einstein–Rosen bridge (wormhole) constructed from the Schwarzschild (AI-)solution between two asymptotically flat universes, one for $\rho > 0$ and the second for $\rho < 0$. The "neck of the bridge" is located at $\rho = 0$.[4]

3.2 The BII-metric

Analogously, it is possible to extend the BII-metrics. In particular, the metric (8) with $\Lambda = 0$, $\epsilon_2 = -1$ and $\epsilon_0 = 1$ (to avoid superficial coordinate singularities in q) is

$$\mathrm{d}s^2 = -p^2(1+q^2)\,\mathrm{d}t^2 + \frac{p^2}{1+q^2}\,\mathrm{d}q^2 + \Big(\frac{2n}{p} - 1\Big)\mathrm{d}z^2 + \Big(\frac{2n}{p} - 1\Big)^{-1}\mathrm{d}p^2\,. \tag{28}$$

The allowed ranges of coordinates are $t, q, z \in \mathbb{R}$, $p \in (0, 2n)$. Correct signature requires $n > 0$, and the metric (28) *does not admit flat (Minkowski) limit* given by $n \to 0$. Similarly to (26) we may apply the transformation

$$p = 2n/(1+\rho^2)\,, \qquad q = \sinh z\,, \qquad z = 2n\,\zeta\,, \tag{29}$$

so that the BII-metric (28) becomes

$$\mathrm{d}s^2 = 4n^2\Big[\big(1+\rho^2\big)^{-2}\big(\mathrm{d}z^2 - \cosh^2 z\,\mathrm{d}t^2\big) + \rho^2\mathrm{d}\zeta^2 + 4\big(1+\rho^2\big)^{-4}\mathrm{d}\rho^2\Big]\,, \tag{30}$$

see metric (2–3.48) in [1]. Again, there is no singularity at $\rho = 0$ corresponding to $p = 2n$, while the curvature singularity at $p = 0$ corresponds to $\rho = \infty$. Static analytic extension of the BII-metric is thus easily obtained by considering the full range $\rho \in \mathbb{R}$ in (30).

[3] The original Ehlers and Kundt transformation for $\epsilon_0 = 1$ is $q = \cosh\tau\,\sin\varphi$, $\tanh t = \tanh\tau/\cos\varphi$.

[4] In [15], the extension of the Schwarzchild solution was obtained by $p \equiv r = \rho^2 + 2m$.

3.3 The $BIII$-metric

This is obtained from (8) by setting $\epsilon_2 = 0$, $\epsilon_0 = 1$, $\Lambda = 0$,

$$\mathrm{d}s^2 = -p^2\,\mathrm{d}t^2 + p^2\,\mathrm{d}q^2 + \frac{2n}{p}\,\mathrm{d}z^2 + \frac{p}{2n}\,\mathrm{d}p^2\,, \tag{31}$$

where $t, q, z \in \mathbb{R}$, $p \in (0, \infty)$. Necessarily $n > 0$, and the metric again does not have the Minkowski limit since $n = 0$ is prohibited. As argued in [4,8], it is a special Levi-Civita solution.

4 Global structure and physical interpretation

After establishing that both the AII-metric and the BI-metric represent specific parts of gravitational field generated by a superluminal source (tachyon moving along a spacelike trajectory), it is now necessary to analyze the global structure of such spacetimes and their relation. In particular, we must describe the way in which the AII-metric

$$\mathrm{d}s^2 = \sigma^2(\mathrm{d}\vartheta^2 + \sinh^2\vartheta\,\mathrm{d}\varphi^2) + \Big(1 - \frac{2M}{\sigma}\Big)\mathrm{d}z^2 - \Big(1 - \frac{2M}{\sigma}\Big)^{-1}\mathrm{d}\sigma^2\,, \tag{32}$$

(which is actually the AII-metric (4) with $\epsilon_2 = -1 = \epsilon_0$, $n = M > 0$, $\Lambda = 0$, using $p = \sigma > 0$, $q = \cosh\vartheta$ and $t = z$) is *combined* with the BI-metric

$$\mathrm{d}s^2 = p^2(-\mathrm{d}\tau^2 + \cosh^2\tau\,\mathrm{d}\varphi^2) + \Big(1 - \frac{2M}{p}\Big)\mathrm{d}z^2 + \Big(1 - \frac{2M}{p}\Big)^{-1}\mathrm{d}p^2\,, \tag{33}$$

(which is the BI-metric (8) with $\epsilon_2 = 1$, $\epsilon_0 = -1$, $n = -M$, $\Lambda = 0$, applying $q = \sinh\tau$, $t = \varphi$).

4.1 Weak-field limit

As suggested already by Gott [14], in the weak-field limit $M \to 0$ the curved spacetime around the tachyonic source becomes flat Minkowski spacetime, with the tachyon becoming just a *test particle located along the Z-axis* (identical to z-axis). The flat spacetime is *divided into distinct regions that are separated by the cylindrical surface* $T^2 = X^2 + Y^2$ with Z arbitrary, as shown in Fig. 1.

Region 1 and Region 2 are given by $T^2 > X^2 + Y^2$ with $T > 0$ and $T < 0$, respectively. These are covered by the metric (32) with $M = 0$, namely

$$\mathrm{d}s^2 = \sigma^2(\mathrm{d}\vartheta^2 + \sinh^2\vartheta\,\mathrm{d}\varphi^2) + \mathrm{d}z^2 - \mathrm{d}\sigma^2\,, \tag{34}$$

whose coordinates are related to background Minkowski coordinates as $Z = z$,

$$\begin{aligned} T &= \pm\sigma\,\cosh\vartheta\,, \\ X &= \sigma\,\sinh\vartheta\,\cos\varphi\,, \\ Y &= \sigma\,\sinh\vartheta\,\sin\varphi\,, \end{aligned} \tag{35}$$

so that $T^2 - X^2 - Y^2 = \sigma^2$. Any $\sigma = \text{const.}$ is thus a hyperboloidal surface. Notice however that the coordinate singularity $\sigma = 0$ actually corresponds to

$$T = 0\,, \qquad X = 0 = Y\,, \tag{36}$$

which is just the Z-axis, *the tachyon trajectory.*

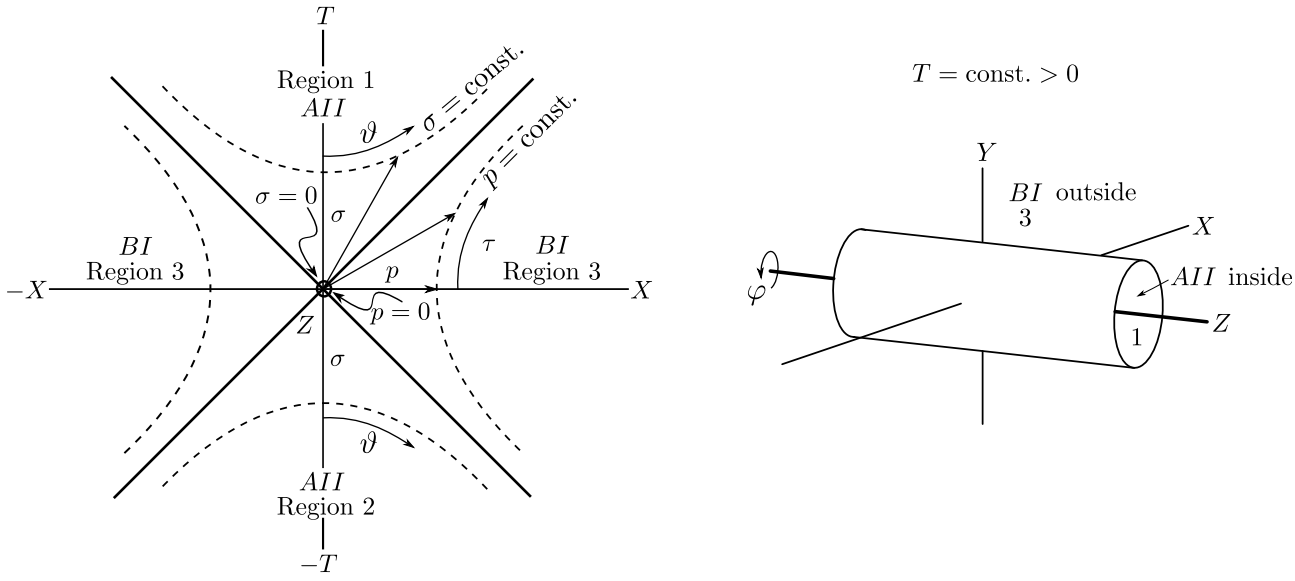

Figure 1: Complete Minkowski spacetime divided into Regions 1 and 2 covered by two "background" AII-metrics (Region 1 for $T > 0$ and Region 2 for $T < 0$) and Region 3 covered by the "background" BI-metric. The left part is the T-X section with $Y = 0$, Z arbitrary, while the right part shows the X, Y, Z subspace with $T = \text{const.} > 0$. For $T > 0$ the boundary is an expanding cylinder whose interior is Region 1, while for $T < 0$ it is a contracting cylinder whose interior is Region 2. Outside this cylinder lies Region 3 covered by the BI-metric. The tachyon moves along the Z-axis with infinite speed.

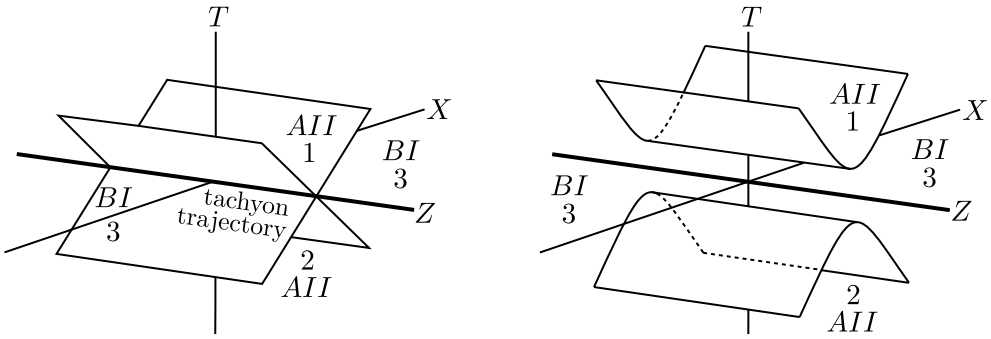

Figure 2: The T, X, Z subspace of Minkowski spacetime for $Y = 0$ (left) and for a constant $Y \neq 0$ (right). It is divided into two disconnected Regions 1 and 2 with the AII-metrics, and one Region 3 with the BI-metric.

Region 3 is defined by $T^2 < X^2 + Y^2$. It is covered by the flat limit of the BI-metric (33)

$$\mathrm{d}s^2 = p^2(-\mathrm{d}\tau^2 + \cosh^2\tau\,\mathrm{d}\varphi^2) + \mathrm{d}z^2 + \mathrm{d}p^2, \tag{37}$$

corresponding to Minkowski coordinates via $Z = z$,

$$\begin{aligned} T &= p\,\sinh\tau\,, \\ X &= p\,\cosh\tau\,\cos\varphi\,, \\ Y &= p\,\cosh\tau\,\sin\varphi\,, \end{aligned} \tag{38}$$

so that $X^2+Y^2-T^2=p^2$. Therefore, $p=\text{const.}$ is a hyperboloidal surface, but the coordinate singularity $p=0$ again corresponds to the line $T=0$, $X=0=Y$, i.e., it is the tachyon trajectory along the Z-axis. It is now also clear that both regions $X>0$ and $X<0$ are covered by taking the full range of the angular coordinate $\varphi\in[0,2\pi)$. Moreover, Region 1 for $Y\neq 0$ is explicitly disconnected from Region 2, see Fig. 2. Thus, two copies of the metric (34) together with the single metric (37) cover the whole Minkowski space (except the separation boundary $X^2+Y^2=T^2$), as shown in Figs. 1 and 2.

4.2 Curved metrics and their analytic extension

Of course, with $M\neq 0$ the complete spacetime covered by pairs of (32) and (33) is not flat anymore. In fact, there is a "tachyonic-type" *curvature singularity* located at $\sigma=0$ for the AII-metric, and formally at $p=0$ for the BI-metric, see (11).

Despite the presence of such curvature singularity, both the metrics *remain asymptotically flat far away from the tachyonic source*, i.e. for σ and p large. Indeed, by inspecting the Cartesian form of the AII-metric (18) it can be observed that for *any finite* X,Y,Z, the metric becomes $\mathrm{d}s^2\approx -\mathrm{d}T^2+\mathrm{d}X^2+\mathrm{d}Y^2+\mathrm{d}Z^2$ as $|T|\to\infty$. The same is true for the BI-metric (20) for *any finite* T and $X^2+Y^2\to\infty$.

There is a coordinate singularity in the AII-metric (32) at $\sigma=2M$. This is clearly the *Killing horizon* generated by the Killing vector ∂_z. For $\sigma>2M$ the coordinate z is spatial, and in this region the metric is time-dependent (σ is a temporal coordinate). On the other hand, for $0<\sigma<2M$ the coordinate z is temporal, and the spacetime region is static (σ is a spatial coordinate). The AII-metric can be maximally analytically extended across $\sigma=2M$, see [14] and Section 9.1.1 of [4] for more details. The corresponding Penrose conformal diagram can be constructed by employing the Kruskal–Szekeres-type coordinates. This is shown in the left part of Fig. 3, and illustrates the null character of the horizons $\sigma=2M$, the timelike character of the curvature singularities $\sigma=0$, and asymptotically flat null infinities $\mathcal{I}^{\pm}$ at $\sigma=\infty$.

Similarly, the BI-metric (33) with $M\neq 0$ ceases to be flat, covering the background exterior region $T^2<X^2+Y^2$ via (38). There is a curvature singularity at $p=0$. However, as explained in Section 3.1, this singularity *can not be reached* because only the range $p\in(2M,\infty)$ is allowed. Instead, the BI-metric can be analytically extended beyond $p=2M$ by performing the transformation $p=2M/(1-\rho^2)$ and taking $\rho\in(-1,1)$, so that the metric becomes

$$\mathrm{d}s^2=4M^2(1-\rho^2)^{-4}\big[\big(1-\rho^2\big)^2\big(-\mathrm{d}\tau^2+\cosh^2\tau\,\mathrm{d}\varphi^2\big)+4\mathrm{d}\rho^2\big]+\rho^2\mathrm{d}z^2\,, \tag{39}$$

cf. (26) and (27). The two distinct asymptotically flat regions $p\to\infty$ for $\rho>0$ and for $\rho<0$ are reached as $\rho\to\pm 1$. These are joined by a "bridge/wormhole" whose "neck" is located at $\rho=0$, corresponding to $p=2M$, where the curvature (11) is maximal but finite. Its geometry is $\mathrm{d}s_2^2=4M^2\left(-\mathrm{d}\tau^2+\cosh^2\tau\,\mathrm{d}\varphi^2\right)$ which is a 2-dimensional de Sitter space.

For fixed values of τ and z, the extended BI-metric (39) reads

$$\mathrm{d}s^2=4M^2(1-\rho^2)^{-4}\big[4\mathrm{d}\rho^2+\big(1-\rho^2\big)^2C^2\mathrm{d}\varphi^2\big]\,, \tag{40}$$

where $C\equiv\cosh\tau\geq 1$ is a constant. *This geometry can be embedded* into three-dimensional Euclidean space with Cartesian coordinates by

$$x_1=\frac{2MC}{1-\rho^2}\cos\varphi\,,\qquad x_2=\frac{2MC}{1-\rho^2}\sin\varphi\,,\qquad x_3=4M\int\frac{\sqrt{1-C^2\rho^2}}{(1-\rho^2)^2}\,\mathrm{d}\rho\,. \tag{41}$$

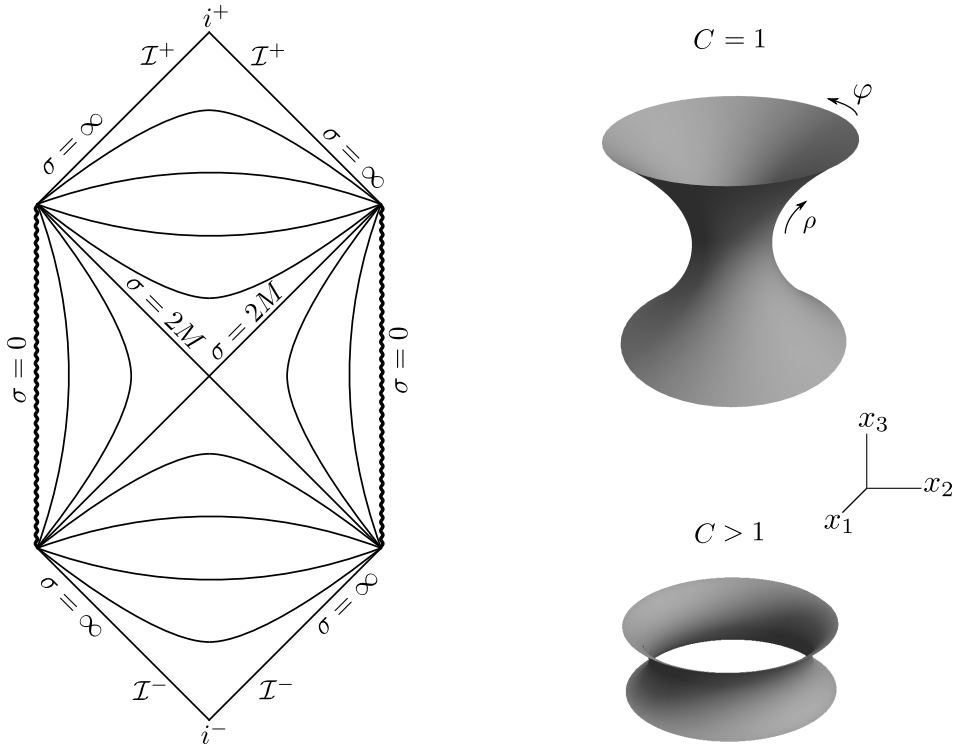

Figure 3: Left: Global conformal diagram for the AII-metric (32) with coordinates ϑ, φ suppressed (in particular, $\vartheta = 0$). Here $i^\pm$ denote past/future timelike infinities, while $\mathcal{I}^\pm$ are null conformal infinities. The horizons $\sigma = 2M$ are null, while the singularities $\sigma = 0$ are timelike. Right: Embedding diagram of the BI-metric (40) for section $z = \text{const.}$ and $\cosh\tau \equiv C = \text{const.}$ For larger C, the neck diameter grows, while the surface becomes more restricted.

For $\tau = 0$, corresponding to $C = 1$, we explicitly obtain $x_3 = 4M\rho/\sqrt{1-\rho^2}$. The embedding surface $x_3^2 = 8M(\sqrt{x_1^2 + x_2^2} - 2M)$, shown in the upper right part of Fig. 3, extends to infinite values of x_i because the whole range $\rho \in (-1, 1)$ is allowed. For $C > 1$ the integral in (41) is more complicated. Numerical integration leads to the axially symmetric embedding surface shown in the lower right part of Fig. 3. As $\tau > 0$ (and thus C) grows, the radius $2MC$ of the neck at $\rho = 0$ grows, while the allowed range of ρ in (41) becomes more restricted to $|\rho| < 1/C$.

4.3 Mach–Cherenkov shockwave separating the AII and BI-metrics

It has been demonstrated in Section 4.1 that, in the weak-field limit $M \to 0$, the complete Minkowski spacetime is covered by two "background" AII-metrics (Regions 1 and 2 for $T > 0$ and $T < 0$, respectively) and one "background" BI-metric (Region 3). These are separated by the *cylindrical surface* $X^2 + Y^2 = T^2$ with Z arbitrary, see Fig. 1. This cylinder *contracts* for $T < 0$ to the Z-axis located at $T = 0$, which is just the tachyon trajectory, and then *re-expands* for $T > 0$. The spacetime region inside this cylinder is covered by the AII-metric, while its exterior is covered by the BI-metric. The cylindrical boundary between them, which contracts/expands at the speed of light to/from the tachyon trajectory, is the *Mach–Cherenkov shockwave generated by the superluminal source*. Since the tachyon moves with *infinite speed*, the "Mach–Cherenkov cone" is "infinitely sharp", i.e., it has a cylindrical geometry.

Of course, with $M \neq 0$ the distinct regions covered by the AII and BI metrics *can not be joined smoothly* across the Mach–Cherenkov surface. While *keeping the cylindrical geometry*, it becomes a surface with *discontinuity* because the specific curvatures on its both sides are different. This gives rise to a *real gravitational shockwave*, whose jump in the curvature can be explicitly evaluated. Instead of using the coordinate representations (32) and (33), this can be explicitly performed in the Cartesian coordinates. Notice that the cylindrical surface $X^2 + Y^2 = T^2$, Z arbitrary, formally degenerates to $\sigma = 0$, $\vartheta = \infty$ in (34) and $p = 0$, $\tau = \infty$ in (37). By combining the AII and BI-metrics in the Cartesian coordinates (18) and (20), it is possible to write a *unified metric for both parts of the curved spacetime* in the whole range of the background coordinates T, X, Y, Z as

$$\mathrm{d}s^2 = -\mathrm{d}T^2 + \mathrm{d}X^2 + \mathrm{d}Y^2 + \mathrm{d}Z^2 \qquad (42)$$
$$+\frac{2M}{\sqrt{|T^2 - X^2 - Y^2|}}\left(-\mathrm{d}Z^2 + \left(1 - \frac{2M}{\sqrt{|T^2 - X^2 - Y^2|}}\right)^{-1} \frac{(-T\mathrm{d}T + X\mathrm{d}X + Y\mathrm{d}Y)^2}{-T^2 + X^2 + Y^2}\right).$$

For $T^2 > X^2 + Y^2$ this is the AII-metric (18) with $M \equiv n$, while for $T^2 < X^2 + Y^2$ this is the BI-metric (20) with $M \equiv -n$.[5] The metric (42) diverges on the shock surface $X^2 + Y^2 = T^2$. In fact, there is an *infinite discontinuity in the Weyl curvature scalar* Ψ_2 (11), namely

$$\Psi_2 = +M\left(T^2 - X^2 - Y^2\right)^{-3/2} \qquad \text{for} \quad T^2 > X^2 + Y^2\,,$$
$$\Psi_2 = -M\left(-T^2 + X^2 + Y^2\right)^{-3/2} \qquad \text{for} \quad T^2 < X^2 + Y^2\,. \qquad (43)$$

The curvature singularity located at the Mach–Cherenkov cylindrical shockwave thus has a specific character such that $\Psi_2 \to +\infty$ when it is approached from its interior, while $\Psi_2 \to -\infty$ when it is approached from its exterior.

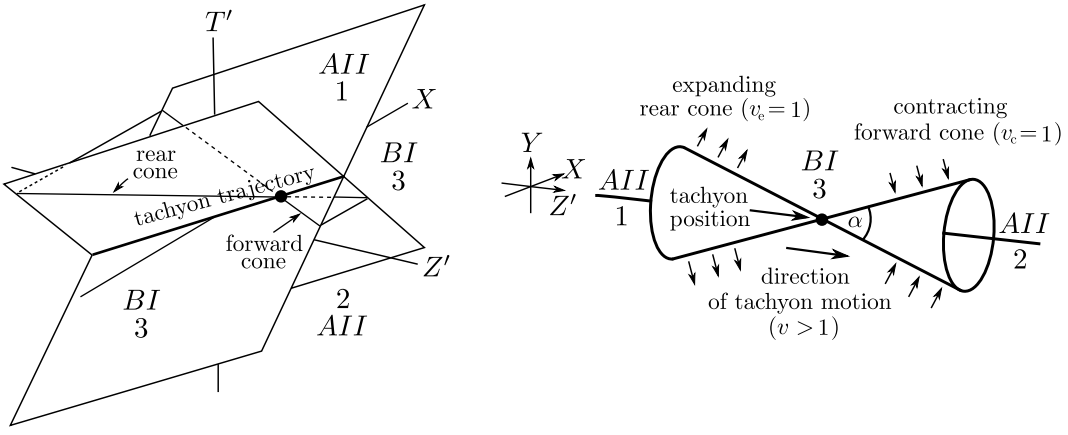

Figure 4: Minkowski spacetime separated into Regions 1, 2, and 3 by the Mach-Cherenkov shock cones generated by the tachyon slowed down by a boost to finite superluminal speed. The spacetime structure is visualized in sections $Y = 0$ (left) and $T' = \text{const.} > 0$ (right). Tachyon moves in the Z'-direction, and generates expanding rear cone and contracting forward cone.

[5] It is natural to choose $M = -n$ to obtain the *same* parameter $M > 0$ for both parts of the unified metric (42). An alternative choice $M = n$ for the BI-metric is mathematically also possible. In such a case the curvature scalar would behave as $\Psi_2 = M\left|T^2 - X^2 - Y^2\right|^{-3/2}$, but the metric on both parts would look different.

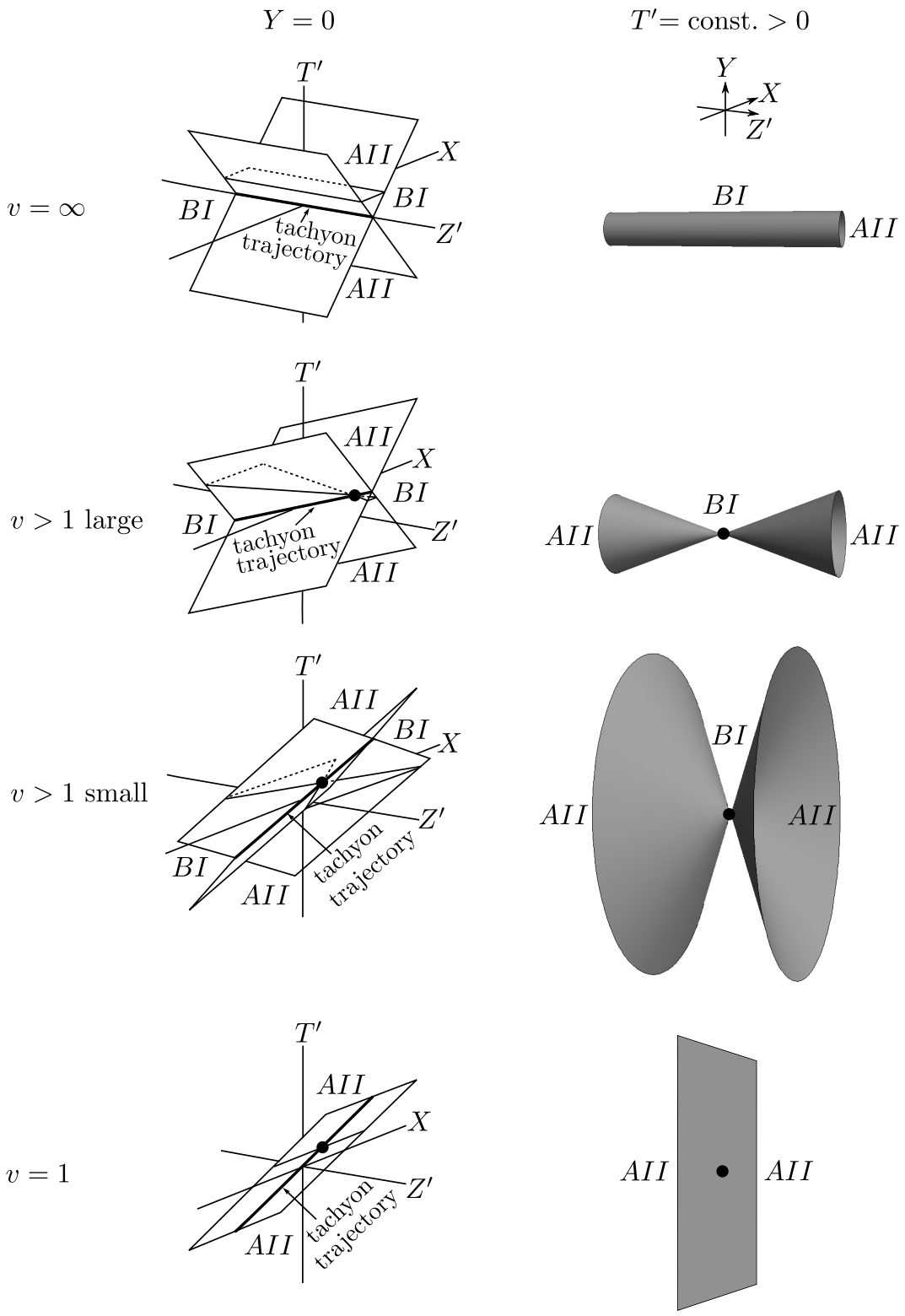

Figure 5: The spacetime structure (left), consisting of the AII and BI-metrics separated by the Mach–Cherenkov shockwaves (right) for various superluminal speeds v of the tachyonic source.

4.4 Boosted metrics

In order to better understand and illustrate the tachyon motion and also the specific character of the generated Mach–Cherenkov cone, it is very convenient to consider a boost of the metric, as originally suggested in [14].

Since the tachyonic source in (34) and (37), and also (32) and (33), moves at *infinite speed* (it is instantaneously located everywhere along on the Z-axis), such a boost will actually *slow it down to finite* superluminal speed $v > 1$. We will use the boost (21). The boosted tachyon then moves in the Z'-direction (coinciding with z') at the speed $v > 1$. In the new coordinates, the surface $\sqrt{X^2 + Y^2} = T$ that separates Regions 1 and 3, and the surface $\sqrt{X^2 + Y^2} = -T$ that separates Regions 2 and 3, take the form

$$X^2 + Y^2 = \frac{(v\,T' - Z')^2}{v^2 - 1}\,. \tag{44}$$

At any fixed time T', these represent *Mach–Cherenkov shock cones with the vertex at* $Z' = v\,T'$ which is the *actual position of the tachyon*, and with the *angle* α of the cone such that $\alpha = 2\,\mathrm{arccot}\sqrt{v^2 - 1}$. As illustrated in Fig. 4, the *rear cone expands* while the *forward cone contracts* at the speed of light. The tachyon is always located at the intersection of these cones and — in a manner similar to the so-called scissors effect — moves faster than light.

It is also illustrative to plot these shockwaves for *different speeds* $v > 1$ of the tachyon, see Fig. 5. For larger superluminal v, the angle α of the cone is smaller. In the extreme case $v = \infty$ this angle is zero and the cone degenerates to the cylinder plotted in Fig. 1, while in the opposite limit $v = 1$ both the rear and front cones coalesce and form a shock plane propagating at the speed of light along Z'. This behavior follows from the dependence of the regions on v. The interior Regions 1 and 2 covered by two separate AII-metrics are located at $X^2 + Y^2 < (v\,T' - Z')^2/(v^2 - 1)$, so that *for smaller superluminal speed* v these regions are *larger*. In the limit $v \to 1$ the whole spacetime (except the Mach–Cherenkov shock, now located at $Z' = T'$) is covered by the pair of AII-metrics. On the other hand, Region 3 defined by $X^2 + Y^2 > (v\,T' - Z')^2/(v^2 - 1)$ becomes *smaller*, and in the limit $v \to 1$ it disappears.

5 AII and BI-metrics with Λ are the Schwarzschild–(anti-)de Sitter spacetime boosted to infinite speed

In previous sections we considered the A and B-metrics in Minkowski background by setting $\Lambda = 0$ in the metrics (4) and (8), respectively. Now we are going to extend the results to any value of the cosmological constant. In fact, we will demonstrate that these metrics can be understood as specific regions of the spacetime representing exact gravitational field of a tachyonic source moving in de Sitter (if $\Lambda > 0$) or anti–de Sitter (if $\Lambda < 0$) universe.

First, let us investigate boosts of the classic Schwarzschild–(anti-)de Sitter metric (which is the most important AI-metric with Λ) and perform the limit $v \to \infty$. However, with $\Lambda \neq 0$ the background is not flat but it is everywhere curved (anti-)de Sitter spacetime. To perform the boost correctly, it is most convenient to employ a five-dimensional embedding formalism. It is well known that (anti-)de Sitter spacetime can be understood as a hyperboloid

$$-\,Z_0^2 + Z_1^2 + Z_2^2 + Z_3^2 + \epsilon Z_4^2 = \epsilon\,a^2\,, \tag{45}$$

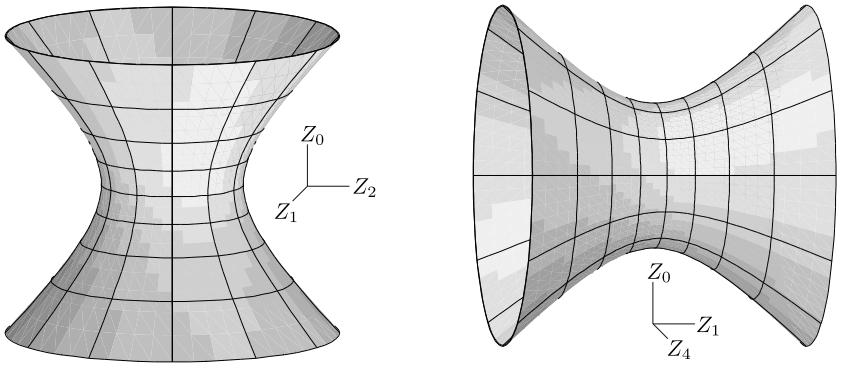

Figure 6: The visualizations of de Sitter spacetime (left) and anti-de Sitter spacetime (right) as hyperboloids (45) embedded in a flat five-dimensional spacetime (46). The remaining coordinates (Z_3, Z_4 for $\Lambda > 0$, and Z_2, Z_3 for $\Lambda < 0$) are suppressed. For more details see [4].

embedded into a five-dimensional flat spacetime

$$\mathrm{d}s^2 = -\mathrm{d}Z_0^2 + \mathrm{d}Z_1^2 + \mathrm{d}Z_2^2 + \mathrm{d}Z_3^2 + \epsilon\,\mathrm{d}Z_4^2\,, \tag{46}$$

where $a \equiv \sqrt{3/|\Lambda|}$ and $\epsilon \equiv \operatorname{sign}\Lambda$, see the visualizations in Fig. 6.

The (anti-)de Sitter background is obtained from the AI-metric (4) for $\epsilon_2 = 1 = \epsilon_0$, $n = 0$. In the case $\Lambda > 0$, these coordinates parametrize the hyperboloid (45) as

$$\left.\begin{aligned} Z_0 &= \pm\sqrt{a^2-p^2}\,\sinh(t/a)\,,\\ Z_1 &= p\,\sqrt{1-q^2}\,\cos\varphi\,,\\ Z_2 &= p\,\sqrt{1-q^2}\,\sin\varphi\,,\\ Z_3 &= p\,q\,,\\ Z_4 &= \pm\sqrt{a^2-p^2}\,\cosh(t/a)\,, \end{aligned}\right\} \text{ for } p<a, \qquad \left.\begin{aligned} Z_0 &= \pm\sqrt{p^2-a^2}\,\cosh(t/a)\,,\\ Z_1 &= p\,\sqrt{1-q^2}\,\cos\varphi\,,\\ Z_2 &= p\,\sqrt{1-q^2}\,\sin\varphi\,,\\ Z_3 &= p\,q\,,\\ Z_4 &= \pm\sqrt{p^2-a^2}\,\sinh(t/a)\,, \end{aligned}\right\} \text{ for } p>a\,, \tag{47}$$

while for $\Lambda < 0$ the corresponding parametrization is

$$\begin{aligned} Z_0 &= \sqrt{a^2+p^2}\,\sin(t/a)\,,\\ Z_1 &= p\,\sqrt{1-q^2}\,\cos\varphi\,,\\ Z_2 &= p\,\sqrt{1-q^2}\,\sin\varphi\,,\\ Z_3 &= p\,q\,,\\ Z_4 &= \sqrt{a^2+p^2}\,\cos(t/a)\,. \end{aligned} \tag{48}$$

Expressing the AI-metric (4) with $\epsilon_2 = 1 = \epsilon_0$ and $n \neq 0$ in these five-dimensional coordinates, using (47), (48), we obtain

$$\mathrm{d}s^2 = \mathrm{d}s^2_{(\mathrm{A})\mathrm{dS}} + \frac{2ma^2}{p}\left(\frac{(Z_4\mathrm{d}Z_0 - Z_0\mathrm{d}Z_4)^2}{(Z_4^2-\epsilon Z_0^2)^2} + \frac{a^2}{p^2}\frac{(Z_0\mathrm{d}Z_0 - \epsilon Z_4\mathrm{d}Z_4)^2}{(Z_4^2-\epsilon Z_0^2)(Z_4^2-\epsilon Z_0^2-2ma^2/p)}\right), \tag{49}$$

where $\mathrm{d}s^2_{(\mathrm{A})\mathrm{dS}}$ is the (anti-)de Sitter background metric (46), $m \equiv -n$ and $p = \sqrt{Z_1^2+Z_2^2+Z_3^2}$. As in [16–18], we can make a boost similar to (14), but now in the coordinates Z_0, Z_3:

$$Z_0 = \frac{Z_0' + v\,Z_3'}{\sqrt{1-v^2}}\,, \qquad Z_3 = \frac{Z_3' + v\,Z_0'}{\sqrt{1-v^2}}\,. \tag{50}$$

We immediately observe that all the terms introducing the factor $\sqrt{1-v^2}$ into (49) are *quadratic*, so it is possible to make the formal limit $v \to \infty$ that will effectively cause just a swap $Z_0^2 \to -Z_3'^2$ and $Z_3^2 \to -Z_0'^2$ in (49). The resulting metric will thus become

$$\mathrm{d}s^2 = \mathrm{d}s^2_{(\mathrm{A})\mathrm{dS}} + \frac{2ma^2}{p}\left(\frac{-(Z_4\mathrm{d}Z_3' - Z_3'\mathrm{d}Z_4)^2}{(Z_4^2+\epsilon Z_3'^2)^2} + \frac{a^2}{p^2}\frac{(Z_3'\mathrm{d}Z_3' + \epsilon Z_4\mathrm{d}Z_4)^2}{(Z_4^2+\epsilon Z_3'^2)(Z_4^2+\epsilon Z_3'^2-2ma^2/p)}\right), \quad (51)$$

where $p = \sqrt{Z_1^2+Z_2^2-Z_0'^2}$. This is the AII-metric in the region $Z_0'^2 > Z_1^2+Z_2^2$ with a purely imaginary mass, and the BI-metric in the region $Z_0'^2 < Z_1^2+Z_2^2$ with a real mass.

Indeed, the AII-metric background (4) for $\epsilon_2 = -1 = \epsilon_0$, $n=0$, with $\Lambda > 0$ is given by

$$\begin{aligned} Z_0 &= p\,q\,,\\ Z_1 &= p\sqrt{q^2-1}\,\cos\varphi\,,\\ Z_2 &= p\sqrt{q^2-1}\,\sin\varphi\,,\\ Z_3 &= \sqrt{p^2+a^2}\,\cos(t/a)\,,\\ Z_4 &= \sqrt{p^2+a^2}\,\sin(t/a)\,, \end{aligned} \quad (52)$$

and with $\Lambda < 0$

$$\left.\begin{aligned} Z_0 &= p\,q\,,\\ Z_1 &= p\sqrt{q^2-1}\,\cos\varphi\,,\\ Z_2 &= p\sqrt{q^2-1}\,\sin\varphi\,,\\ Z_3 &= \pm\sqrt{a^2-p^2}\,\sinh(t/a)\,,\\ Z_4 &= \pm\sqrt{a^2-p^2}\,\cosh(t/a)\,, \end{aligned}\right\} \text{ for } p<a\,, \qquad \left.\begin{aligned} Z_0 &= p\,q\,,\\ Z_1 &= p\sqrt{q^2-1}\,\cos\varphi\,,\\ Z_2 &= p\sqrt{q^2-1}\,\sin\varphi\,,\\ Z_3 &= \pm\sqrt{p^2-a^2}\,\cosh(t/a)\,,\\ Z_4 &= \pm\sqrt{p^2-a^2}\,\sinh(t/a)\,, \end{aligned}\right\} \text{ for } p>a\,. \quad (53)$$

These parametrizations only cover the region $Z_0^2 > Z_1^2+Z_2^2$. The complete AII-metric with $n \neq 0$ written in the coordinates of (52), (53) thus has the form

$$\mathrm{d}s^2 = \mathrm{d}s^2_{(\mathrm{A})\mathrm{dS}} + \frac{2na^2}{p}\left(\frac{-(Z_4\mathrm{d}Z_3 - Z_3\mathrm{d}Z_4)^2}{(Z_4^2+\epsilon Z_3^2)^2} - \frac{a^2}{p^2}\frac{(Z_3\mathrm{d}Z_3 + \epsilon Z_4\mathrm{d}Z_4)^2}{(Z_4^2+\epsilon Z_3^2)(Z_4^2+\epsilon Z_3^2-2na^2/p)}\right), \quad (54)$$

where $p = \sqrt{Z_0^2-Z_1^2-Z_2^2}$. We clearly see that this is exactly the Schwarzschild–(anti-)de Sitter metric (51) boosted to infinite speed, with the identification $m = \mathrm{i}\,n$ (and $p^2 \to -p^2$).

Similarly, the BI-metric (8) for $\epsilon_2 = 1$, $\epsilon_0 = -1$, $n=0$ corresponds to the parametrization

$$\left.\begin{aligned} Z_0 &= p\,q\,,\\ Z_1 &= p\sqrt{1+q^2}\,\cos t\,,\\ Z_2 &= p\sqrt{1+q^2}\,\sin t\,,\\ Z_3 &= \sqrt{a^2-p^2}\,\cos(z/a)\,,\\ Z_4 &= \sqrt{a^2-p^2}\,\sin(z/a)\,, \end{aligned}\right\} \text{ for } \Lambda>0\,, \qquad \left.\begin{aligned} Z_0 &= p\,q\,,\\ Z_1 &= p\sqrt{1+q^2}\,\cos t\,,\\ Z_2 &= p\sqrt{1+q^2}\,\sin t\,,\\ Z_3 &= \pm\sqrt{a^2+p^2}\,\sinh(z/a)\,,\\ Z_4 &= \pm\sqrt{a^2+p^2}\,\cosh(z/a)\,, \end{aligned}\right\} \text{ for } \Lambda<0\,, \quad (55)$$

which only covers the region $Z_0^2 < Z_1^2+Z_2^2$. In terms of the coordinates (55), the complete BI-metric reads

$$\mathrm{d}s^2 = \mathrm{d}s^2_{(\mathrm{A})\mathrm{dS}} + \frac{2na^2}{p}\left(\frac{(Z_4\mathrm{d}Z_3' - Z_3'\mathrm{d}Z_4)^2}{(Z_4^2+\epsilon Z_3'^2)^2} - \frac{a^2}{p^2}\frac{(Z_3'\mathrm{d}Z_3' + \epsilon Z_4\mathrm{d}Z_4)^2}{(Z_4^2+\epsilon Z_3'^2)(Z_4^2+\epsilon Z_3'^2+2na^2/p)}\right), \quad (56)$$

which is again the same as the Schwarzschild–de Sitter metric boosted to infinite speed (51) with $m=-n$ and $p = \sqrt{Z_1^2+Z_2^2-Z_0^2}$.

We may thus conclude that *both* the AII and BI-metrics with any Λ can be understood as (formal) *limits of the classic Schwarzschild–(anti-)de Sitter metric boosted to infinite speed*. Of course, complementary procedures can also be applied: the Schwarzschild-de Sitter metric can be obtained by slowing down (stopping) the source of the AII-metric with imaginary mass, or the BI-metric with real mass.

6 Coordinate ranges and extensions of the B-metrics with $\Lambda \neq 0$

To understand the global character of the B-metrics with any cosmological constant, and their possible extensions and combinations, it is necessary to analyze the admitted coordinate ranges.

6.1 BI-metric with Λ

For $\epsilon_2 = 1$ the metric (8) is

$$\mathrm{d}s^2 = -p^2(\epsilon_0 - q^2)\,\mathrm{d}t^2 + \frac{p^2}{\epsilon_0 - q^2}\,\mathrm{d}q^2 + \Big(1 + \frac{2n}{p} - \frac{\Lambda}{3}\,p^2\Big)\mathrm{d}z^2 + \Big(1 + \frac{2n}{p} - \frac{\Lambda}{3}\,p^2\Big)^{-1}\mathrm{d}p^2\,. \quad (57)$$

The coordinate ranges are (considering $\epsilon_0 = -1$) $q, z \in \mathbb{R}$, $t \in [0, 2\pi)$, while the range of p depends on n and Λ. It is determined by the roots of the cubic equation

$$-\frac{\Lambda}{3}\,p^3 + p + 2n = 0\,. \quad (58)$$

The best way to illustrate the allowed ranges of $p > 0$ for all possible cases is to plot the possible roots p_i of (58) as intersections of the function $-\frac{\Lambda}{3}\,p^3 + p$ with horizontal lines corresponding to various values of $-2n$. Since the metric coefficients g_{zz} and g_{pp} must remain positive, we require $-\frac{\Lambda}{3}\,p^3 + p > -2n$. Explicit visualization is given in Fig. 7. The left part applies to $\Lambda > 0$, the right part to $\Lambda < 0$. It can be seen that for $\Lambda > 0$ and $n \geq 0$, the values of p are $p \in (0, p_1)$. For $-\frac{1}{3\sqrt{\Lambda}} < n < 0$, the allowed range is $p \in (p_0, p_1)$ given by two roots of (58). For $n = -\frac{1}{3\sqrt{\Lambda}}$ the metric degenerates because only one value $p = \frac{1}{\sqrt{\Lambda}}$ is allowed. Finally, there is no solution for $n < -\frac{1}{3\sqrt{\Lambda}}$. In the case $\Lambda < 0$, the situation is much simpler because the function $-\frac{\Lambda}{3}\,p^3 + p$ monotonously grows from zero. Therefore, for $n \geq 0$ the coordinate p takes the maximal range $(0, \infty)$, while for $n < 0$ its range is restricted to $p \in (p_0, \infty)$.

Interestingly, it is possible to analytically extend the BI-metric (57) across p_i (the roots of g_{zz}) by performing the transformation

$$\rho^2 = 1 + \frac{2n}{p} - \frac{\Lambda}{3}p^2\,, \qquad \sinh\tau = q\,, \qquad \zeta = \frac{1}{2n}\,z\,, \qquad \varphi = t\,. \quad (59)$$

In fact, for $\Lambda = 0$ this reduces to (26). The resulting metric is

$$\mathrm{d}s^2 = 4n^2\Big[R_1(\rho)\big(-\mathrm{d}\tau^2 + \cosh^2\tau\,\mathrm{d}\varphi^2\big) + \rho^2\mathrm{d}\zeta^2 + R_2(\rho)\,\mathrm{d}\rho^2\Big]\,, \quad (60)$$

where $R_1(\rho) = \frac{1}{4n^2}\,p^2(\rho)$, $R_2(\rho) = \frac{1}{4n^2}\left(n\,p(\rho)^{-2} + \frac{1}{3}\Lambda\,p(\rho)\right)^{-2}$, with $p(\rho)$ obtained by inverting the relation (59). For $\Lambda = 0$ we recover the metric (27). Relations between the ranges of p and the ranges of $\rho > 0$ are shown in Table 2. Analytic extension across $\rho = 0$ is obtained by admitting a "mirror chart" with $\rho < 0$.

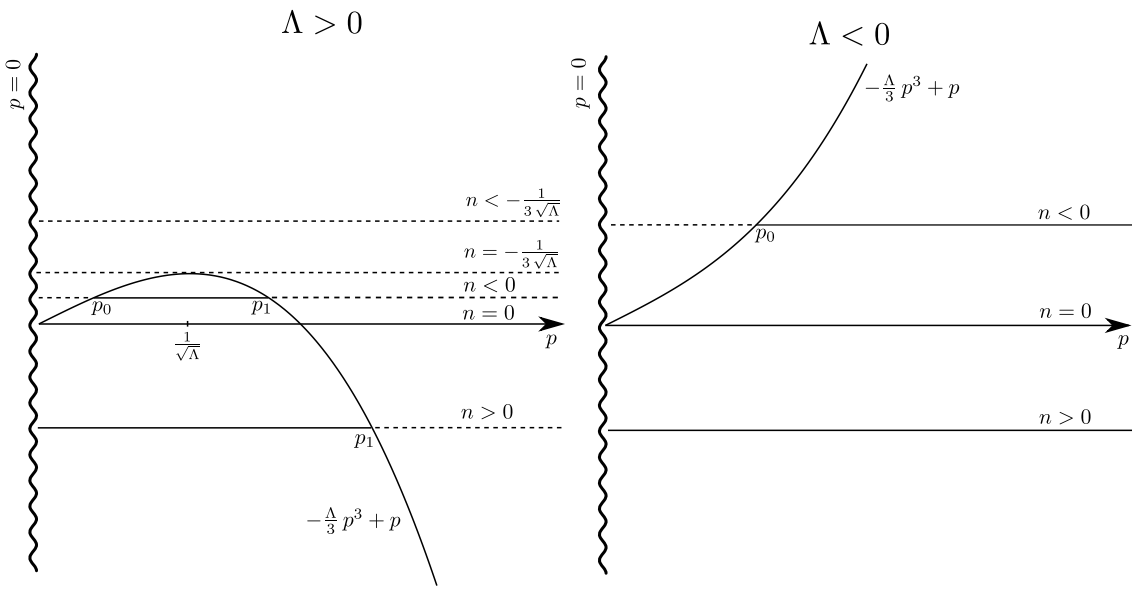

Figure 7: Allowed ranges of the coordinate p for $\Lambda > 0$ (left) and $\Lambda < 0$ (right) in the BI-metric (57). The horizontal lines correspond to different values of $-2n$. The parts of these lines that lie under the curve $-\frac{\Lambda}{3}\,p^3 + p$ determine the admitted range of p. Their parts above the curve are dashed — there is no solution for these values because the metric would no longer have the correct signature. The intersections mark the roots p_0, p_1 of (58), with $0 < p_0 < p_1$.

Λ	n	range of p	range of $\rho > 0$
> 0	> 0	$(0, p_1)$	$(0, \infty)$
> 0	< 0	(p_0, p_1)	$(0, \rho_{\max})$
< 0	> 0	$(0, \infty)$	$(\rho_{\min}, \infty)$
< 0	< 0	(p_0, ∞)	$(0, \infty)$

Table 2: Ranges of p and the corresponding ranges of ρ for possible combinations of Λ and n in the BI-metric (57). Here $\rho_{\min}$ and $\rho_{\max}$ denote specific minimal and maximal values or ρ.

6.2 BII-metric with Λ

For $\epsilon_2 = -1$ the metric (8) gives

$$\mathrm{d}s^2 = -p^2(\epsilon_0 + q^2)\,\mathrm{d}t^2 + \frac{p^2}{\epsilon_0 + q^2}\,\mathrm{d}q^2 + \Big(-1 + \frac{2n}{p} - \frac{\Lambda}{3}\,p^2\Big)\mathrm{d}z^2 + \Big(-1 + \frac{2n}{p} - \frac{\Lambda}{3}\,p^2\Big)^{-1}\mathrm{d}p^2\,, \quad (61)$$

where $t, q, z \in \mathbb{R}$ (considering $\epsilon_0 = 1$). The range of p is given by the roots $0 < p_0 < p_1$ of

$$-\frac{\Lambda}{3}\,p^3 - p + 2n = 0\,. \quad (62)$$

We plot the allowed ranges of p for different values of Λ and n in Fig. 8. For $\Lambda > 0$, $n > 0$ the range is $p \in (0, p_0)$, while the case $n \leq 0$ is forbidden. For $\Lambda < 0$ the coordinate p has the full range $(0, \infty)$ for any $n > \frac{1}{3\sqrt{|\Lambda|}}$. If $n = \frac{1}{3\sqrt{|\Lambda|}}$ the metric degenerates at $p = \frac{1}{\sqrt{|\Lambda|}}$. If $0 < n < \frac{1}{3\sqrt{|\Lambda|}}$, the metric represents two separate regions $p \in (0, p_0)$ and $p \in (p_1, \infty)$. Finally,

if $n \leq 0$ the coordinate p can only take values $p \in (p_1, \infty)$. Notice that $n \leq 0$ is forbidden for the BII-metric (28) with $\Lambda = 0$ and (61) with $\Lambda > 0$. In particular, the BII-metric (61) with $\Lambda < 0$ (and sufficiently large $|\Lambda|$) includes the anti–de Sitter spacetime when $n = 0$.

Again, we can perform its analytic extension across p_i, in this case by generalizing (29) to

$$\rho^2 = -1 + \frac{2n}{p} - \frac{\Lambda}{3} p^2 \,, \qquad \sinh z = q \,, \qquad \zeta = \frac{1}{2n}\, z \,. \tag{63}$$

The extended BII-metric will then be

$$\mathrm{d}s^2 = 4n^2 \Big[R_1(\rho) \big(\mathrm{d}z^2 - \cosh^2 z \, \mathrm{d}t^2 \big) + \rho^2 \mathrm{d}\zeta^2 + R_2(\rho) \, \mathrm{d}\rho^2 \Big] \,. \tag{64}$$

Explicit form of the metric functions $R_1(\rho), R_2(\rho)$ (reducing to (30) when $\Lambda = 0$) is obtained by using the function $p(\rho)$ that is obtained by inverting expression (63). The ranges of $\rho > 0$ corresponding to the allowed ranges of p are shown in Table 3.

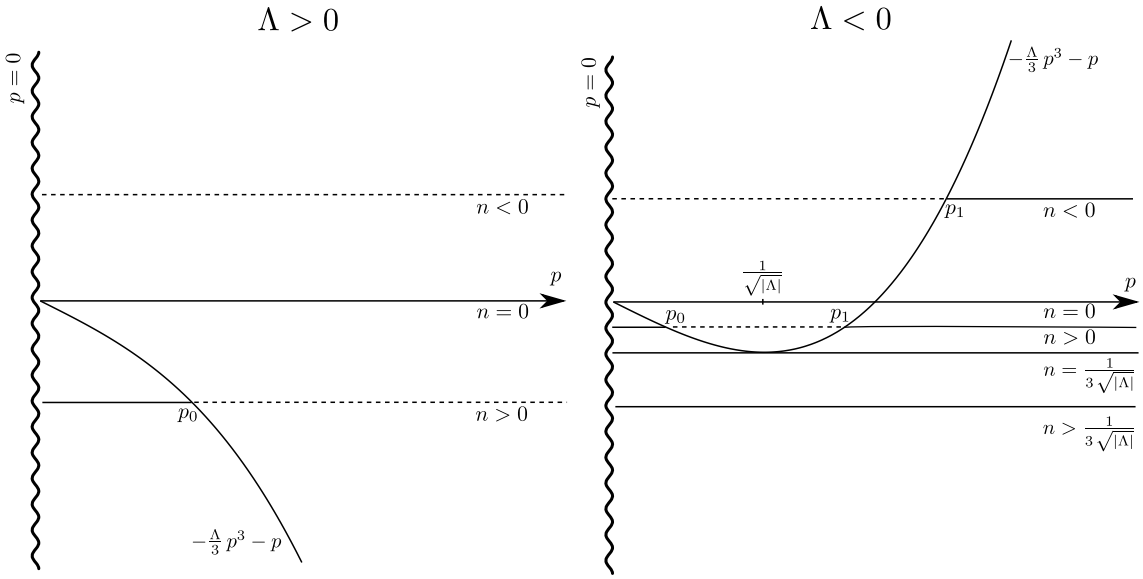

Figure 8: Allowed ranges of p for $\Lambda > 0$ (left) and $\Lambda < 0$ (right) in the BII-metric (61). They are determined by those parts of the horizonal lines $-2n$ that lie under the curve $-\frac{\Lambda}{3}\, p^3 - p$.

Λ	n	range of p	range of $\rho > 0$
> 0	> 0	$(0, p_0)$	$(0, \infty)$
< 0	$> \frac{1}{3\sqrt{\lvert\Lambda\rvert}}$	$(0, \infty)$	$(\rho_{\min}, \infty)$
< 0	$0 < n < \frac{1}{3\sqrt{\lvert\Lambda\rvert}}$	$(0, p_0), (p_1, \infty)$	$(0, \infty)$
< 0	< 0	(p_1, ∞)	$(0, \infty)$

Table 3: Ranges of p and ρ for possible Λ and n in the BII-metric (61).

6.3 $BIII$-metric with Λ

The metric (8) for $\epsilon_2 = 0$ (and, without loss of generality, $\epsilon_0 = 1$) reads

$$\mathrm{d}s^2 = -p^2\,\mathrm{d}t^2 + p^2\,\mathrm{d}q^2 + \Big(\frac{2n}{p} - \frac{\Lambda}{3}\,p^2\Big)\mathrm{d}z^2 + \Big(\frac{2n}{p} - \frac{\Lambda}{3}\,p^2\Big)^{-1}\mathrm{d}p^2\,, \tag{65}$$

where $t, q, z \in \mathbb{R}$, and the range of p is determined by the roots of

$$-\frac{\Lambda}{3}p^3 + 2n = 0\,. \tag{66}$$

The results are visualized in Fig. 9. For $\Lambda > 0$, $n > 0$, the allowed range is $p \in (0, p_0)$. As for the BII-metric, the case $n \le 0$ is not allowed. When $\Lambda < 0$, $n \ge 0$, the coordinate p take the whole range $(0, \infty)$, while for $n < 0$, it takes (p_0, ∞). Of course, equation (66) can be explicitly solved: For $n/\Lambda > 0$, the root is $p_0 = \sqrt[3]{6n/\Lambda}$, while for $n/\Lambda < 0$ there is no positive root. These $BIII$-metrics are, in fact, equivalent to the Linet–Tian metric, see [8, 19].

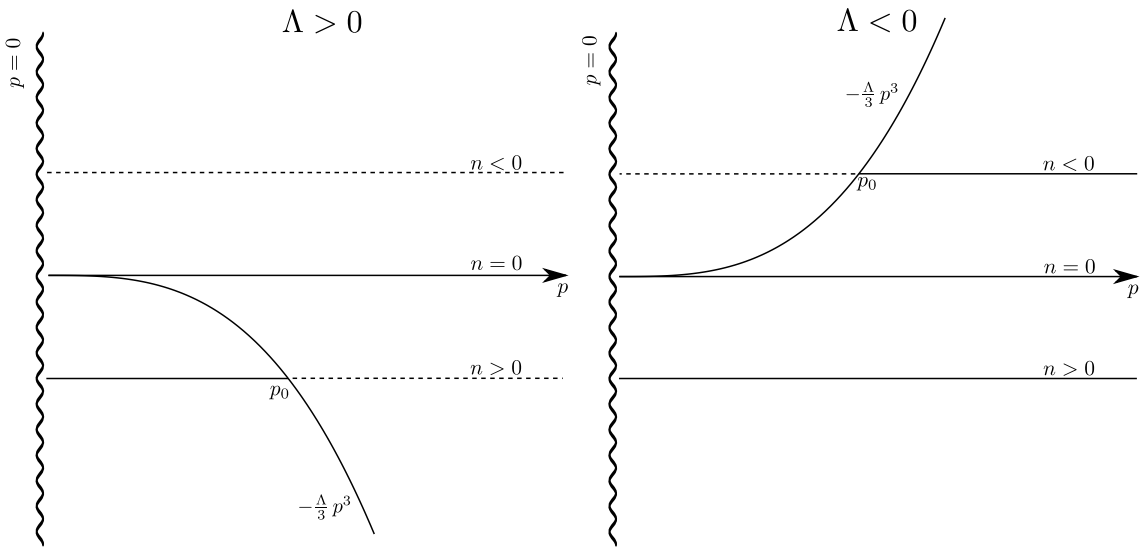

Figure 9: Allowed ranges of p for $\Lambda > 0$ (left) and $\Lambda < 0$ (right) in the $BIII$-metric (65). They are determined by the root $p_0 = \sqrt[3]{6n/\Lambda}$ of (66).

Λ	n	range of p	range of $\rho > 0$
> 0	> 0	$(0, p_0)$	$(0, \infty)$
< 0	> 0	$(0, \infty)$	$(\rho_{\min}, \infty)$
< 0	< 0	(p_0, ∞)	$(0, \infty)$

Table 4: Ranges of p and ρ for possible Λ and n in the $BIII$-metric (65).

We can also make an analytic extension beyond p_0 (which does not have a counterpart for the $\Lambda = 0$ case because there are no roots of g_{zz}). Such an extension is achieved by

$$\rho^2 = \frac{2n}{p} - \frac{\Lambda}{3}p^2\,, \qquad \zeta = \frac{1}{2n}\,z\,, \tag{67}$$

and the extended $BIII$-metric takes the form

$$\mathrm{d}s^2 = 4n^2\Big[R_1(\rho)\big(-\mathrm{d}t^2+\mathrm{d}q^2\big)+\rho^2\mathrm{d}\zeta^2+R_2(\rho)\,\mathrm{d}\rho^2\Big]\,, \tag{68}$$

where $R_1(\rho)$, $R_2(\rho)$ are evaluated by inverting (67). The allowed ranges of p and the corresponding ranges of ρ are summarized in Table 4.

7 Global structure and physical interpretation: tachyons in (anti-)de Sitter spacetime

The metric describing both internal Regions 1 and 2 around the tachyonic source is the AII-metric with Λ, namely

$$\mathrm{d}s^2 = \sigma^2(\mathrm{d}\vartheta^2+\sinh^2\vartheta\,\mathrm{d}\varphi^2)+\Big(1-\frac{2M}{\sigma}+\frac{\Lambda}{3}\,\sigma^2\Big)\mathrm{d}z^2-\Big(1-\frac{2M}{\sigma}+\frac{\Lambda}{3}\,\sigma^2\Big)^{-1}\mathrm{d}\sigma^2\,, \tag{69}$$

while the external Region 3 is described by the BI-metric with Λ

$$\mathrm{d}s^2 = p^2(-\mathrm{d}\tau^2+\cosh^2\tau\,\mathrm{d}\varphi^2)+\Big(1-\frac{2M}{p}-\frac{\Lambda}{3}\,p^2\Big)\mathrm{d}z^2+\Big(1-\frac{2M}{p}-\frac{\Lambda}{3}\,p^2\Big)^{-1}\mathrm{d}p^2\,, \tag{70}$$

generalizing (32) and (33).

7.1 Weak-field limit and distinct regions

As for $\Lambda = 0$, the key point is to consider the weak-field limit $M \to 0$ of (69) and (70), in which case the curvature singularities at $\sigma = 0$ and $p = 0$ disappear and the spacetimes (being then vacuum and conformally flat) can readily be interpreted as (anti-)de Sitter universe in which the *test tachyonic source* (located at $\sigma = 0$ and $p = 0$) moves with infinite speed.

The trajectory of such tachyon on the hyperboloid (45) can be determined using the corresponding five-dimensional parametrizations. The internal AII-metric (69) with $M = 0$ and $\Lambda > 0$ is de Sitter spacetime covered by

$$\begin{aligned} Z_0 &= \pm\sigma\,\cosh\vartheta\,,\\ Z_1 &= \sigma\,\sinh\vartheta\,\cos\varphi\,,\\ Z_2 &= \sigma\,\sinh\vartheta\,\sin\varphi\,,\\ Z_3 &= \sqrt{\sigma^2+a^2}\,\cos\phi\,,\\ Z_4 &= \sqrt{\sigma^2+a^2}\,\sin\phi\,, \end{aligned} \tag{71}$$

which is actually (52) with $p = \sigma > 0$, $q = \pm\cosh\vartheta$ and $t = z \equiv a\,\phi$. The coordinate singularity at $\sigma = 0$ with ϑ finite, localizing the test tachyon, thus corresponds to the trajectory

$$\begin{aligned} &Z_0 = 0\,, \qquad Z_1 = 0 = Z_2\,,\\ &Z_3 = a\,\cos\phi\,,\\ &Z_4 = a\,\sin\phi\,. \end{aligned} \tag{72}$$

Unlike the tachyon in Minkowski space whose trajectory is given by the straight line (36), which is the Z-axis, this tachyon *runs at infinite speed around the neck of the de Sitter hyperboliod*,

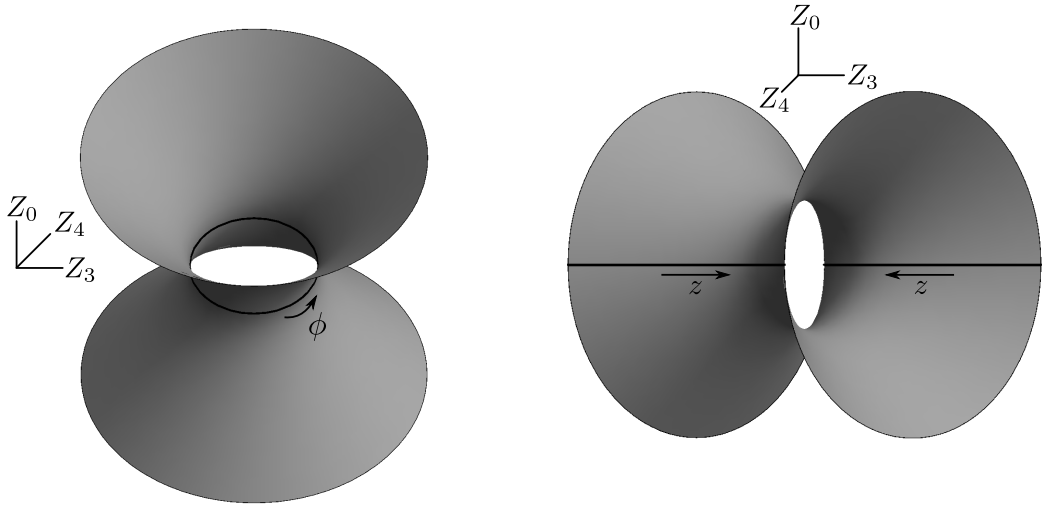

Figure 10: Motion of the infinitely fast test tachyon in (anti-)de Sitter background space. For $\Lambda > 0$, the tachyon runs with infinite speed in closed circle around the neck of the de Sitter hyperboloid (left). For $\Lambda < 0$, there are two tachyons running along two hyperbolic lines on opposite sides, corresponding to the signs $\pm$ in (75), of the anti-de Sitter hyperboloid (right).

which is the smallest possible circle $Z_3^2 + Z_4^2 = a^2$ in such a closed universe, see the left part of Fig. 10.

The same is true for the external BI-metric (70) with $M = 0$ and $\Lambda > 0$. Indeed, the corresponding parametrization is

$$\begin{aligned} Z_0 &= p\,\sinh\tau\,, \\ Z_1 &= p\,\cosh\tau\,\cos\varphi\,, \\ Z_2 &= p\,\cosh\tau\,\sin\varphi\,, \\ Z_3 &= \sqrt{a^2-p^2}\,\cos\phi\,, \\ Z_4 &= \sqrt{a^2-p^2}\,\sin\phi\,, \end{aligned} \tag{73}$$

equivalent to (55) with $q = \sinh\tau$, $t = \varphi$ and $z = a\,\phi$. Setting $p = 0$ at finite τ, we obtain again the tachyonic trajectory (72).

For $\Lambda < 0$ the tachyonic trajectory is different. The anti-de Sitter hyperboloid (45) with $\epsilon = -1$ is parametrized in the form of the (weak-field limit of) the AII-metric (69) as

$$\begin{aligned} Z_0 &= \pm\sigma\,\cosh\vartheta\,, \\ Z_1 &= \sigma\,\sinh\vartheta\,\cos\varphi\,, \\ Z_2 &= \sigma\,\sinh\vartheta\,\sin\varphi\,, \\ Z_3 &= \pm\sqrt{a^2-\sigma^2}\,\sinh(z/a)\,, \\ Z_4 &= \pm\sqrt{a^2-\sigma^2}\,\cosh(z/a)\,, \end{aligned} \tag{74}$$

cf. (53). The test tachyon trajectory given by $\sigma = 0$ with ϑ finite is thus located at

$$\begin{aligned} &Z_0 = 0\,, \qquad Z_1 = 0 = Z_2\,, \\ &Z_3 = \pm a\,\sinh(z/a)\,, \\ &Z_4 = \pm a\,\cosh(z/a)\,. \end{aligned} \tag{75}$$

There are thus *two* tachyons *moving at infinite speed along main hyperbolic lines* $Z_4^2 - Z_3^2 = a^2$ *on opposite sides of the anti-de Sitter hyperboloid*, as illustrated on the right part of Fig. 10.

The same result is obtained for the BI-metric (70), which for $\Lambda < 0$ corresponds to

$$\begin{aligned} Z_0 &= p \sinh\tau\,, \\ Z_1 &= p \cosh\tau \cos\varphi\,, \\ Z_2 &= p \cosh\tau \sin\varphi\,, \\ Z_3 &= \pm\sqrt{a^2+p^2}\,\sinh(z/a)\,, \\ Z_4 &= \pm\sqrt{a^2+p^2}\,\cosh(z/a)\,, \end{aligned} \tag{76}$$

see (55). For $p = 0$ and finite τ, we recover the same tachyonic trajectory (75).

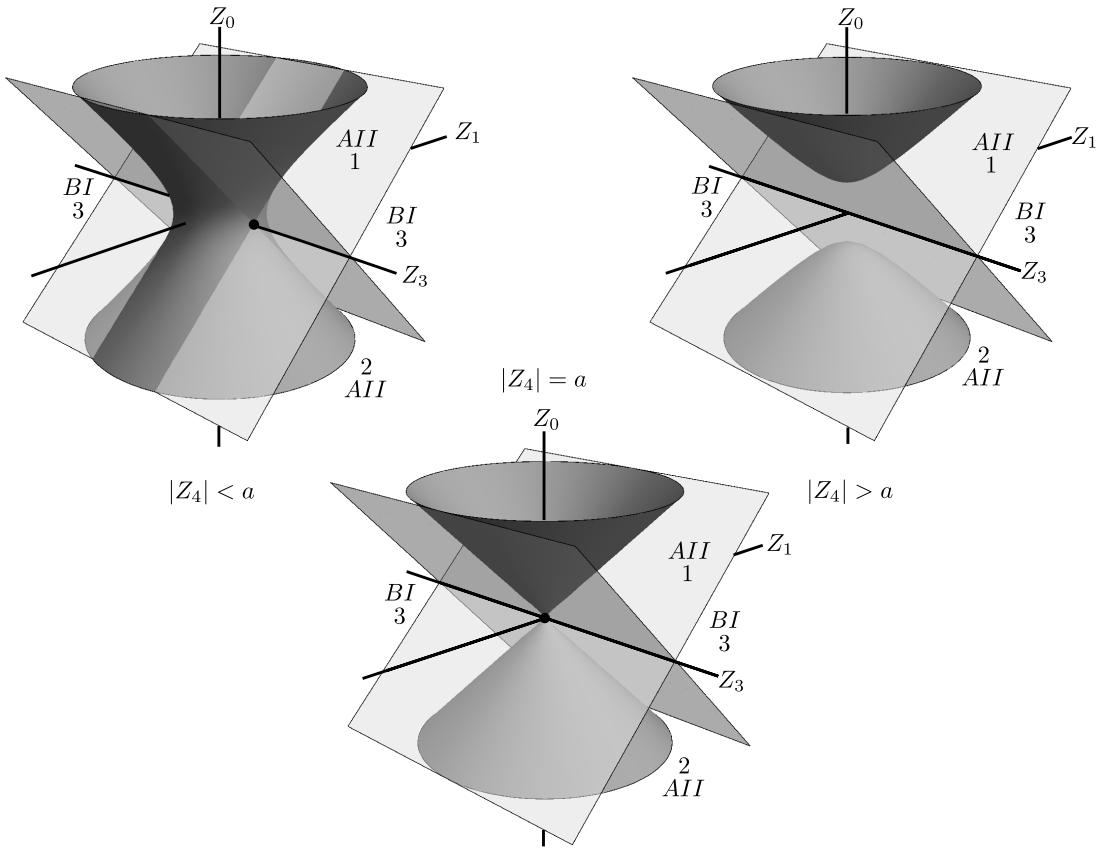

Figure 11: Separation of the background de Sitter space into Regions 1, 2 and 3, covered by the AII and BI-metrics, for $Z_2 = 0$ and $|Z_4| < a$ (upper left part), $|Z_4| > a$ (upper right part) and $|Z_4| = a$ (lower part). For $|Z_4| < a$ the separation surface $Z_1^2 + Z_2^2 = Z_0^2$ cuts the de Sitter hyperboloid, for $|Z_4| = a$ it is tangent to it, and for $|Z_4| > a$ this surface does not intersect the hyperboloid. Because the coordinate Z_4 is suppressed here, the tachyon motion is not visualized very well: In this section, it corresponds just to two points at the intersection of the Z_3-axis with the hyperboloid when $|Z_4| < a$, and one point when $|Z_4| = a$. The tachyon motion is better seen in Fig. 10 where both nontrivial coordinates Z_3 and Z_4 are visible.

7.2 Mach–Cherenkov shockwave separating the AII and BI-metrics

In the weak-field limit, a pair of metrics (69) and (70) together cover the full (anti-)de Sitter universe. Internal Region 1 and Region 2 are localized at $Z_0^2 > Z_1^2 + Z_2^2$ with $Z_0 > 0$ and $Z_0 < 0$, respectively. They are represented by two AII-metrics (69). The complementary external Region 3 represented by a single BI-metric (70) is localized at $Z_0^2 < Z_1^2 + Z_2^2$.

These regions are *separated by the surface* $Z_1^2 + Z_2^2 = Z_0^2$, with Z_3 arbitrary such that $Z_3^2 = \epsilon(a^2 - Z_4^2)$, corresponding to the singularity $\sigma = 0, \vartheta = \infty$ and $p = 0, \tau = \infty$, respectively. This surface represents the *Mach–Cherenkov shocks*, the *contracting one for* $Z_0 < 0$ given by $\sqrt{Z_1^2 + Z_2^2} = -Z_0$ and the *expanding one for* $Z_0 > 0$ given by $\sqrt{Z_1^2 + Z_2^2} = Z_0$. As in the case of Minkowski background, visualized in Fig. 1, it is locally a *contracting/expanding cylinder around the superluminal tachyonic source*. However, in the $\Lambda > 0$ case, this cylinder is "wraped" around the circular trajectory (72) in closed de Sitter space, so that topologically and also geometrically it is a *toroidal surface*. For $\Lambda < 0$, instead, there are *two infinite cylinders* around (75) on opposite sides of the anti-de Sitter hyperbolic space, see Fig. 10.

The position of these shock surfaces, separating the AII and BI regions, is shown in Fig. 11 for typical three-dimensional sections (given by three distinct values of Z_4) through de Sitter space, and in Fig. 12 for anti-de Sitter space.

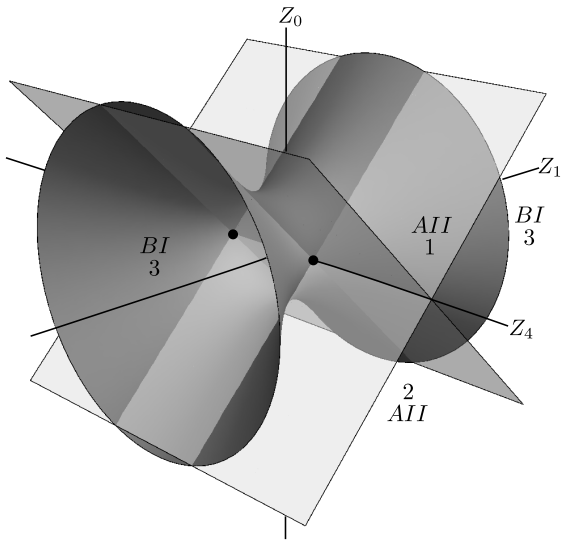

Figure 12: Separation of the background anti-de Sitter space into Regions 1, 2 and 3 for the section $Z_2 = 0$ with $Z_3 = \text{const}$. Unlike for de Sitter space, visualized in Fig.11, this picture looks qualitatively the same for any value of Z_3. Motion of the tachyon is better seen in Fig. 10.

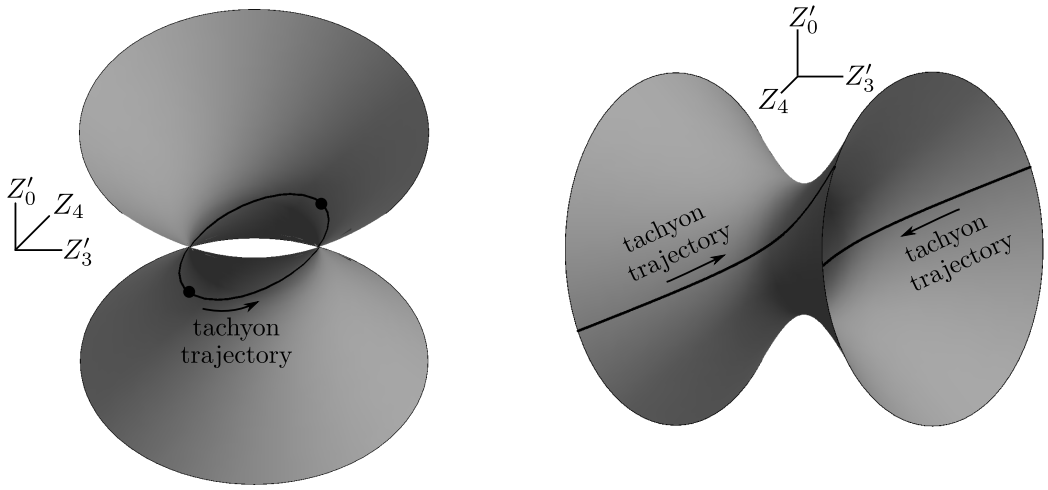

Figure 13: Motion of a slowed tachyon in de Sitter (left) and anti-de Sitter (right) background space in boosted coordinates. Its trajectory is given by $Z'_3/Z'_0 = v > 1$ and $Z_1 = 0 = Z_2$.

7.3 Boosted metrics with $\Lambda \neq 0$

Following the idea outlined in [7], it is useful to perform a *boost which slows the tachyonic source* from infinite speed to some finite speed $v > 1$. This enables us to better illustrate its motion and the generated Mach–Cherenkov conical shockwaves in (anti-)de Sitter universe, analogously to flat background case shown in Fig. 4. Such a boost must be performed in the 5-dimensional coordinates of (45), (46). Choosing the spatial Z_3-direction, it reads

$$Z_0 = \frac{v\,Z'_0 - Z'_3}{\sqrt{v^2-1}}\,, \qquad Z_3 = \frac{v\,Z'_3 - Z'_0}{\sqrt{v^2-1}}\,, \tag{77}$$

cf. (21). The tachyon moving along $Z_1 = 0 = Z_2$ at $Z_0 = 0$, see (72), (75), is then located at $Z'_3 = v\,Z'_0$, and the shockwave surface $Z_1^2 + Z_2^2 = Z_0^2$ becomes

$$Z_1^2 + Z_2^2 = \frac{(v\,Z'_0 - Z'_3)^2}{v^2-1}. \tag{78}$$

The *trajectory* of thus slowed tachyon in (anti-)de Sitter universe is illustrated in Fig. 13.

Such a motion in de Sitter space admits two interpretations. Either the tachyon moves forward in time from the initial point (starting at $Z'_0 = -Z'_{0\,\max}$) to the final point (reaching it at $Z'_0 = +Z'_{0\,\max}$), and then travels *backwards in time* to the initial point, also at speed faster than light. Alternatively, the tachyon moves from the initial to the final point along *both trajectories* (recall that there is not a unique geodesic between two events in pseudo-Riemannian geometry). The specific value $Z'_{0\,\max}$ can be evaluated. Substituting the conditions $Z_1 = 0 = Z_2$, $Z'_3 = v\,Z'_0$ into the boosted form of (45), namely $-Z_0'^2 + Z_1^2 + Z_2^2 + Z_3'^2 + Z_4^2 = a^2$, we obtain $Z_0'^2 = (a^2 - Z_4^2)/(v^2-1)$. This explicitly determines the position of the tachyon on the de Sitter hyperboloid as a function of time Z'_0. Extreme values of Z'_0 arise when $Z_4 = 0$, yielding

$$Z'_{0\,\max} = \frac{a}{\sqrt{v^2-1}}\,. \tag{79}$$

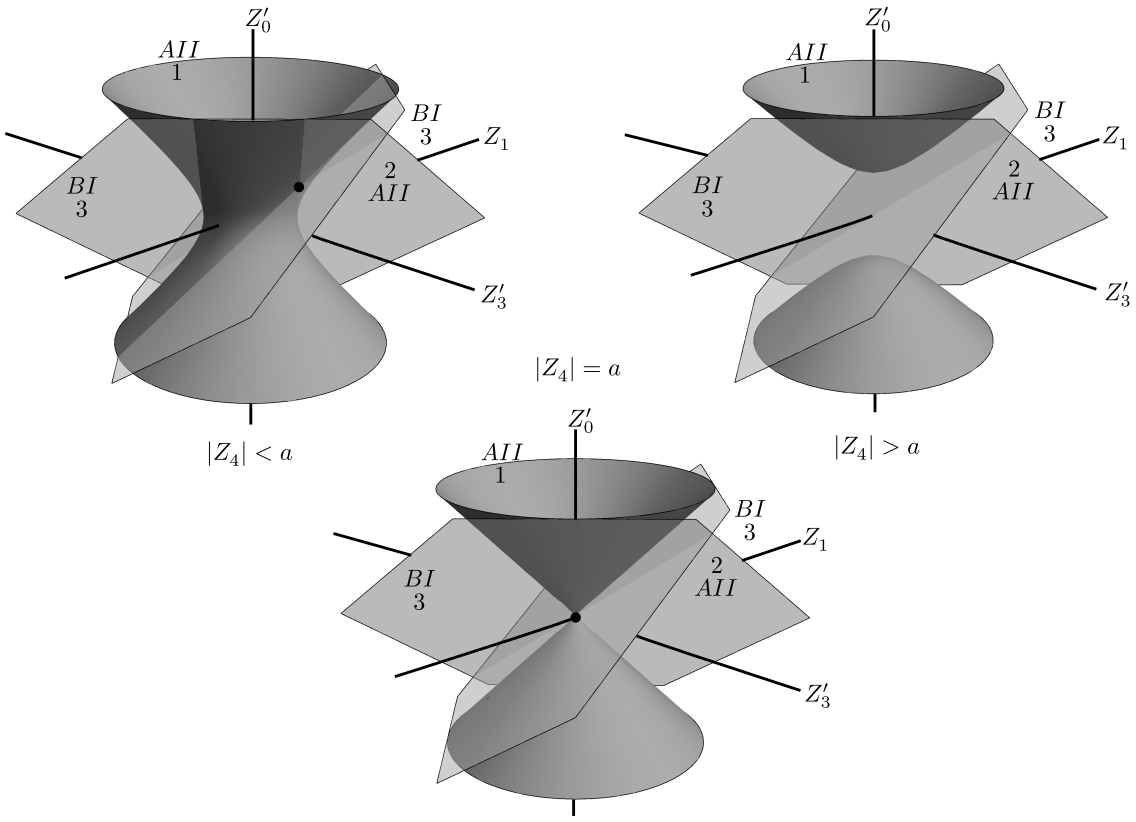

Figure 14: Separation of de Sitter universe into Regions 1, 2 and 3 in the boosted coordinates for $|Z_4| < a$ (upper left part), $|Z_4| > a$ (upper right part) and $|Z_4| = a$ (lower part), with $Z_2 = 0$. The intersections of these separation boundaries with the hyperboloid in the upper left part give the position of the Mach–Cherenkov shock cones in de Sitter universe. The tachyon is always located at their joint vertex at $Z_1 = 0 = Z_2$.

In anti-de Sitter space there are *two tachyons*, each moving faster than light on the opposite sides of the universe, see the right part of Fig. 13. "Unfolding" the hyperboloid, there would be just one tachyon oscillating between $Z'_3, Z_4 = \pm\infty$, that is "bouncing off" the conformal infinity.

Visualization of Regions 1, 2 and 3, separated by the conical shockwave surface (78) in the *boosted coordinates of de Sitter space*, is shown in Fig. 14. At any time Z'_0, this separation boundaries localize on the hyperboloid the Mach–Cherenkov shock, namely the *rear expanding cone* and the *forward contracting cone*. Analogously as in the situation shown in Fig. 4, the tachyon is always located at the intersection of these two cones at $Z_1 = 0 = Z_2$.

Similarly, in Fig. 15 we visualize these separation boundaries and the corresponding two conical shocks in the *boosted form of anti-de Sitter space*.

Finally, it is illustrative to visualize de Sitter spacetime, together with the actual position of the Mach–Cherenkov shocks, in *spatial sections* given by Z_1, Z_2, Z'_3 (with a fixed value of $Z_4 < a$). This is done in Fig. 16 for five different times $Z'_0 = \text{const}$. In any such section, the de Sitter spatial geometry is a 3-sphere, represented here as a 2-sphere because one spatial dimension is suppressed in this plot. As a function of Z'_0, this *de Sitter sphere contracts*

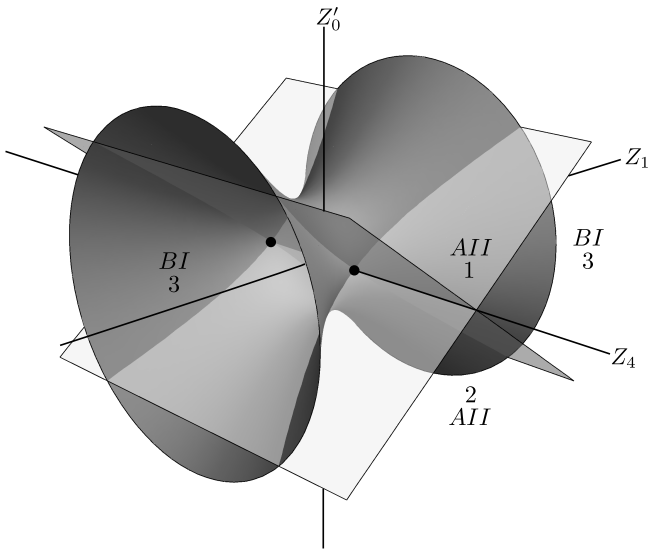

Figure 15: Separation of anti-de Sitter universe into Regions 1, 2 and 3 in the boosted coordinates. Notice that Regions 1 and 2, covered by the AII-metrics, are larger, whereas Region 3 covered by the BI-metric is smaller, compared to Fig. 12 (i.e., without the boost).

to a minimal size at $Z'_0 = 0$ *and then re-expands*. The shock surface given by (78) has the form of two cones, with the tachyon located at their joint vertex. The position of the Mach–Cherenkov shocks in de Sitter universe is given here by the *circular intersection of these cones with each sphere*. There are two shocks, the forward shock and the rear one. Recall that these shocks separate the internal Regions 1 and 2 (with the AII-metric) from the external Region 3 (endowed with the BI-metric).

The top left part of Fig. 16 shows the situation in a generic time $Z'_0 < -Z'_{0\,\max}$, in which case both the shocks are contracting from the equator of the spherical de Sitter space, approaching the North Pole and the South pole (both located at $Z_1 = 0 = Z_2$), respectively. At the special time $Z'_0 = -Z'_{0\,\max}$, shown in the top right part, the tachyon occurs in the North Pole of the space when the first contracting shock reaches it, crosses it, and starts to re-expand. The second shock on the southern hemisphere continues to contract towards the South pole. At $Z'_0 = 0$, see the middle part of Fig. 16, the situation is fully symmetric: The closed de Sitter universe has a minimal radius, both shock waves are of the same size, and are located symmetrically with respect to the equator. For $Z'_0 > 0$, the situation is complementary to the top part of the figure. Bottom left part shows the tachyon located in the South Pole at time $Z'_0 = Z'_{0\,\max}$ when the second contracting shock has just shrinked to zero and starts to re-expand from the South Pole, while the first shock had been already expanding from the North Pole. A generic situation at a time $Z'_0 > Z'_{0\,\max}$ is shown in the bottom right part of Fig. 16, with two expanding shocks in the expanding de Sitter universe, both of them approaching the equator.

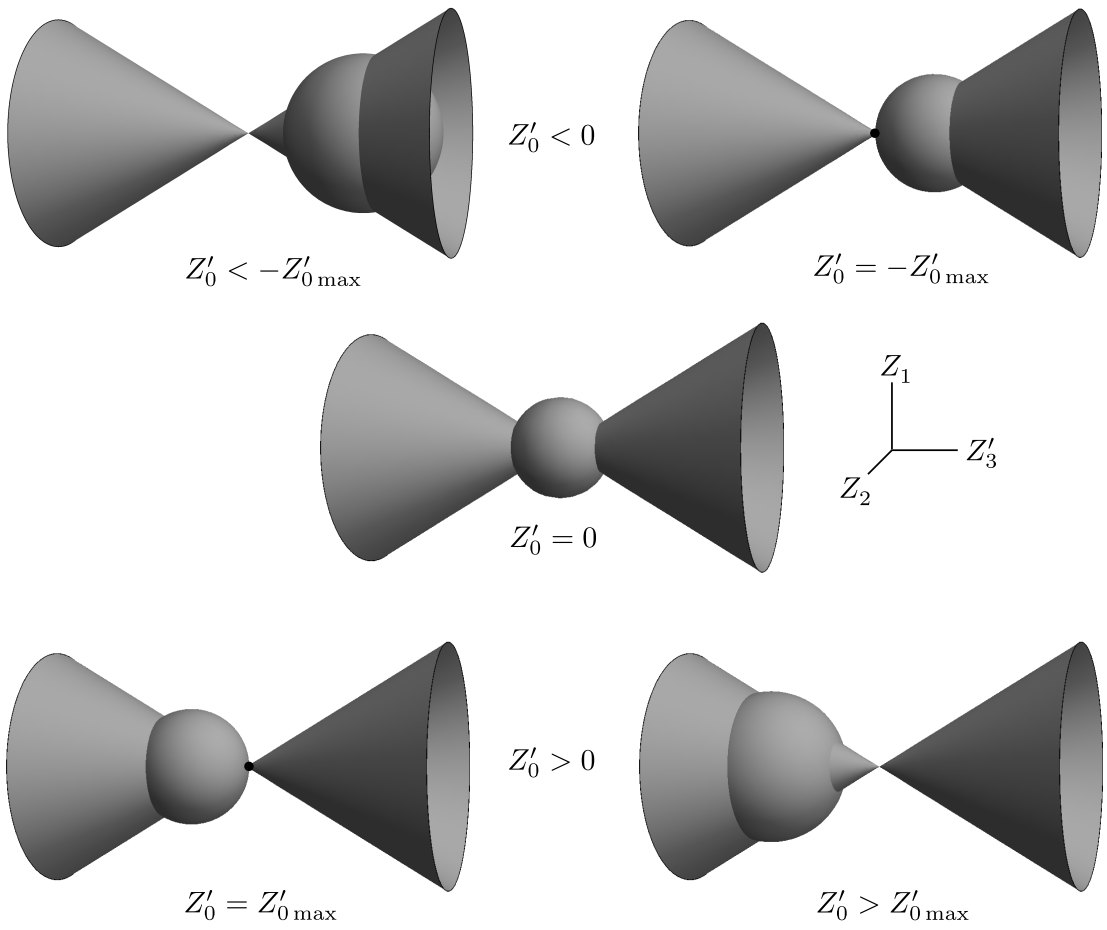

Figure 16: A time sequence visualizing de Sitter universe — in this section Z_1, Z_2, Z'_3 represented as a sphere — at five different times $Z'_0 = \text{const.}$ (and fixed $Z_4 < a$). The universe contracts, reaches its minimal size at $Z'_0 = 0$, and then re-expands. The intersections of the sphere with the cones give the actual position of the two Mach–Cherenkov shocks in the universe. For $Z'_0 < -Z'_{0\,\max}$ both shocks are contracting on the sphere towards its Poles, while for $Z'_0 > Z'_{0\,\max}$ they are both expanding from the Poles. The tachyon is always located at the joint vertex of the cones. Analogous pictures apply to anti-de Sitter universe expressed in global static coordinates because the 2-spaces of constant T and r are also spheres, see the metric (5.4) in [4].

8 Conclusions

We have presented and analyzed the classes of A and B-metrics with an arbitrary value of the cosmological constant. While the famous Schwarzschild–(anti-)de Sitter spacetime (which is the AI-metric) represents the spherically symmetric gravitational field of a static massive source, the AII and BI-metrics describe the field of a superluminal source, i.e. tachyon moving along the axis of symmetry. In fact, all these three families of metrics are related by an appropriate boost (admitting speeds $v > 1$).

We have studied the weak-field limit, analytic extensions, and global structure of these

spacetimes. We have demonstrated that the full gravitational field of a tachyon in Minkowski or (anti-)de Sitter universe is obtained by combining a pair of AII-metrics with a single BI-metric. The former represent the contracting/expanding interior regions while the latter represents an exterior region with respect to the separation boundary which is the contracting/expanding Mach–Cherenkov shockwave. This structure of the "composite spacetime", yielding the complete gravitational field of a tachyon moving with any superluminal speed in Minkowski, de Sitter or anti-de Sitter universe, has been analyzed and visualized on numerous pictures.

In fact, the present work is the third paper in our recent series which we have devoted to deeper geometric, algebraic, and physical investigation of a large family on non-expanding Plebański–Demiański space-times. This whole family, generalizing the original B-metrics of [1], was described and its free parameters were identified and studied in our work [8]. A thorough investigation of the character of the corresponding background coordinates for de Sitter and anti-de Sitter universe was presented in [7]. We hope that, together with this third complementary paper, we have thus provided an extensive survey and review of this simple yet interesting family of exact solutions of Einstein's field equations.

Acknowledgements

This work was supported by the Czech Science Foundation grant GAČR 17-01625S. O.H. also acknowledges the support by the Charles University Grant GAUK 196516.

References

[1] Ehlers, J. and Kundt, W. (1962). Exact solutions of the gravitational field equations, in *Gravitation: An introduction to current research* (Wiley, New York), 49–101.

[2] Kinnersley, W. and Walker, M. (1970). Uniformly accelerating charged mass in general relativity, *Phys. Rev. D* **2**, 1359–70.

[3] Stephani, H., Kramer, D., MacCallum, M., Hoenselaers , C. and Herlt, E. (2003). *Exact solutions of Einstein's field equations, 2nd edition* (Cambridge University Press, Cambridge).

[4] Griffiths, J. B. and Podolský, J. (2009). *Exact Space-Times in Einstein's General Relativity* (Cambridge University Press, Cambridge).

[5] Schwarzschild, K. (1916). Über das Gravitationsfeld eines Massenpunktes nach der Einsteinschen Theorie, *Sitz. Preuss. Akad. Wiss. Berlin*, 189–196. English translation: (2003) *Gen. Rel. Grav.* **35**, 951–9.

[6] Kottler, F. (1918). Über die physikalischen Grundlagen der Einsteinschen Gravitationstheorie, *Ann. Physik* **56** (361), 401–62.

[7] Podolský, J. and Hruška, O. (2017). Yet another family of diagonal metrics for de Sitter and anti-de Sitter spacetimes. *Phys. Rev. D* **95**, 124052 (29pp).

[8] Podolský, J., Hruška, O. and Griffiths, J. B. (2018). Non-expanding Plebański–Demiański space-times, *Class. Quantum Grav.* **35**, 165011 (35pp).

[9] Plebański, J. F. and Demiański, M. (1976). Rotating charged and uniformly accelerating mass in general relativity, *Ann. Phys.* **98**, 98–127.

[10] Griffiths, J. B. and Podolský, J. (2006). A new look at the Plebański–Demiański family of solutions. *Int. J. Mod. Phys. D* **15**, 335–69.

[11] Hruška, O. (2015). The study of exact spacetimes with a cosmological constant. Diploma Thesis, Charles University, Faculty of Mathematics and Physics, Prague (193pp).

[12] Peres, A. (1970). Gravitational field of a tachyon, *Physics Letters A* **31**, 361–2.

[13] Schulman, L. S. (1971). Gravitational shock waves from tachyons. *Nuovo Cimento B* **2**, 38–44.

[14] Gott, J. R. (1974). Tachyon singularity: A spacelike counterpart of the Schwarzschild black hole, *Nuovo Cimento B* **22**, 49–69.

[15] Einstein, A. and Rosen, N. (1935). The particle problem in the general theory of relativity. *Phys. Rev.* **48**, 73–7.

[16] Hotta, M. and Tanaka, M. (1993). Shock-wave geometry with non-vanishing cosmological constant, *Class. Quantum Grav.* **10**, 307–14.

[17] Podolský, J. and Griffiths, J. B. (1997). Impulsive gravitational waves generated by null particles in de Sitter and anti-de Sitter backgrounds, *Phys. Rev. D* **56**, 4756–67.

[18] Podolský, J. and Griffiths, J. B. (1998). Boosted static multipole particles as sources of impulsive gravitational waves, *Phys. Rev. D* **58**, 124024 (5pp).

[19] Griffiths, J. B. and Podolský, J. (2010). The Linet–Tian solution with a positive cosmological constant in four and higher dimensions, *Phys. Rev. D* **81**, 064015 (6pp).